ELECTRICAL RESISTIVITY IMAGING FOR CHARACTERIZATION OF COAL BEARING LAYERS AT ODAGBO VILLAGE, KOGI STATE, NIGERIA

BY

EUGENE ANIBE IDOGBE

DEPARTMENT OF PHYSICS,
FACULTY OF PHYSICAL SCIENCES,
AHMADU BELLO UNIVERSITY,
ZARIA, NIGERIA

MAY, 2021

ELECTRICAL RESISTIVITY IMAGING FOR CHARACTERIZATION OF COAL BEARING LAYERS AT ODAGBO VILLAGE, KOGI STATE, NIGERIA

BY

EUGENE ANIBE IDOGBE,
BSC PHYSICS (ABU) 2014
P16PSPY8018

A THESIS SUBMITTED TO THE SCHOOL OF POSTGRADUATE STUDIES, AHMADU BELLO UNIVERSITY, ZARIA

IN PARTIAL FULFILLMENT OF THE REQUIREMENTS FOR THE AWARD OF MASTER OF SCIENCE DEGREE IN APPLIED GEOPHYSICS

DEPARTMENT OF PHYSICS,
FACULTY OF PHYSICAL SCIENCES,
AHMADU BELLO UNIVERSITY,
ZARIA, NIGERIA

MAY, 2021

DECLARATION

I declare that the work in this thesis entitled Electrical Resistivity Imaging for Characterization of Coal Bearing Layers at Odagbo Village, Kogi State, Nigeria has been performed by me in the department of PHYSICS under the supervision of Dr. A. L. Aminu and Prof. K. M. Lawal. The information derived from the literature has been duly acknowledged in the text and a list of references provided. No part of this thesis was previously presented for another degree or diploma at this or any other institution.

Eugene Anibe IDOGBE	_____	_____
Name of Student	Signature	Date

CERTIFICATION

This thesisentitledELECTRICAL RESISTIVITY IMAGING FOR CHARACTERIZATION OF COAL BEARING LAYERS AT ODAGBO VILLAGE, KOGI STATE, NIGERIA by EUGENE ANIBE IDOGBE meets the regulation governing the award of the degree of MASTER OF SCIENCE in APPLIED GEOPHYSICS of the Ahmadu Bello University, and is approved for its contribution to knowledge and literary presentation.

Dr. A. L. Aminu	_____	_____
Chairman, Supervisory Committee	Signature	Date
Prof. K. M. Lawal	_____	_____
Member, Supervisory Committee	Signature	Date
Prof. Rabiu Nasiru	_____	_____
Head of Department	Signature	Date
Prof. Sani Abdullahi	_____	_____
Dean, School of Postgraduate Studies	Signature	Date

ACKNOWLEDGEMENT

I am indeed grateful to Almighty God for his guidance and protection from the start and conclusion of my MSc. Programme.

I am thankful to my supervisors, Dr. A.L. Ahmed and Prof. K.M. Lawal for their tutelage; technical guidance, constructive comments, critical reading and directions, and assistance. I want to thank the Head of Department of Physics, Prof. Rabiu Nasiru, P.G. coordinator, Dr. N.N Garba, Seminar coordinator, Dr. A.A. Khaleed, Coordinator Applied Geophysics unit, Dr. R. Jimoh, and Chief Technologist, Mal. Sani for their efforts in ensuring a successful running of the M.Sc. progamme throughout the period of my study.

I want to thank the Head of the Department of Physics, University of Abuja, for his assistance with the equipment used for this research.

I appreciate the efforts of my lecturers, Prof. K.M. Lawal, Dr. P. Sule, Dr. A.L. Ahmed, Dr. J. Raimi, and Dr. J. Osumeje, for the quality knowledge of Geophysics they exposed me to. Also, I appreciate Dr. S.S. Magaji, Dr. Y. Abubakar, Dr. Lawal, Prof. S.A. Alagbe, and other lecturers in Geology for their intellectual contribution via quality knowledge of Geology they exposed me to ensure the actualization of the work.

To my parents, Mr. Basil I. Idogbe and Mrs. Victoria T. Idogbe, and my siblings who sponsored this progamme, I pray God will reward them abundantly.

Special thanks to my colleagues, seniors, and all who have supported me in various ways to my completion of this programme. I wish you all success in your future endeavours.

DEDICATION

This research work is dedicated to my parents Mr. and Mrs. Basil I. Idogbe and my beloved siblings.

ABSTRACT

Coal is considered as a vital energy mix that build the bedrock of energy access and bridge the energy demand gaps between different countries of the world. The search for Coal at an old mine working in Odagbo village is being carried out by artisan miners who indiscriminately dig underground tunnels in search of Coal.This approach is imprecise, laborious, and harmful to miners and may create geohazards that affect the community and potential coal resources.Electrical resistivity imaging was carried out at a mining site in Odagbo village Kogi state, Nigeria. The research aimed to characterize Coal seam within the study area. The study was targeted at determining the resistivity value associated with the Coal seam and the probable depth of the Coal seam. The LUND imaging system consisting of the ABEM Terrameter SAS 4000, electrode selector ES 464, stainless-steel electrodes, multi-core cables, and jumpers were used to acquire the data in this study. The protocol chosen was the dipole-dipole array because of its supreme sensitivity to; resistivity variation below the electrode in each dipole pair, horizontal variation of resistivity, and to 3D structures. Data processing was done using RES2DINV software. The result of the resistivity imaging revealed three layers of earth materials closely related to resistivity values at a depth of about 30 m from the ground surface. The first layer had resistivity values averagely greater than 700 Ωm. The second layer had resistivity values lower than 2200 Ωm. This layer is probably the host of the coal seam. The third layer had resistivity values greater than 700 Ωm. Coal seams are probably more at the North-East of the survey area and the coal seam is suspected to have resistivity values ranging from about 67 Ωm to 549 Ωm and depth varying from 12 m to 25 m.

TABLE OF CONTENTS

LIST OF FIGURES

LIST OF TABLES

LIST OF PLATES

CHAPTER ONE

INTRODUCTION

1.1 Background to the Study

Energy is an essential facet of development, yet, the world is faced with twin energy-related challenges: one of energy insufficiency and affordability, and the other of energy inefficiency and environmentally friendly to meet economic development and population growth. As an effect, many countries use different types of energy mix such as crude oil, natural gas, coal, nuclear, hydroelectricity, and alternatives such as solar radiation and wind to meet an increasing trend of global energy demand. Hence, there is a growing search for sustainable energy access targets that balances the crisis between development and the environment.

Coal is considered as a vital energy mix that build the bedrock of energy access and bridge the energy demand gaps between different countries of the world (Board, 2009; Khatib, 2012) This is because, it is readily combustible organic rock (Schopf, 1956), and is one of the earth's resources found in abundance and widely distributed around the world with reserves of about 990 billion tons for all types of coal available for consumption (Brown, 2012). Its attractive attributes stimulated man's principal research interest in Coal (Aja & Emeribe 2000; Ward, 2003; Gupta, 2007; Tsikritzis *et al.*, 2008) for exploitation and usage domestically and globally. Coal consumption has grown to fuel 42% of global electricity production (Birol, 2008). Countries like Poland, South Africa, China, and Australia rely on Coal for over 94%, 92%, 77%, and 76% of their electricity respectively (Board, 2012). Coal is probable to remain an indispensable component of the energy mix to complement a range of energy sources such as oil and gas reserves and nuclear energy for sustainable

energy future, especially in developing countries (Board, 2009; Miller, 2011; Oji *et al*., 2012; Schnapp& Smith, 2012; Mills, 2014; Cozzi & Gould, 2015; Oberschelp*et al*., 2019).

In Nigeria, Coal was first discovered in Udi near Enugu in 1909 (Borishade *et al*., 1985; Famuboni, 1996; Obaje *et al.*, 1996; Obaje & Hamza, 2000; Ogala *et al.*, 2005;Michael *et al.*, 2008; Olayande *et al.*, 2012; Ogala, 2018), and its extensive exploration reported an economic estimate of about 639 million tons proven reserves and about 2.8 billion tons inferred reserves distributed over some States (MMSD, 2006; Obaje, 2009; Mallo, 2012; Sada 2012; Christine, 2015), but mostly within the Benue Trough geological province (Kogbe, 1976). Onakoya*et al*., (2013)stated that Nigerian coal consists of about 49% sub-bituminous, 39% bituminous, and 12% lignite coals within coalfields of two main groups: the Turonian-Coniacian and the Campano-Maastrichtian coals. According toAgagu & Ekweozor, (1982), Orajaka *et al.*, (1990), Akande *et al.*, (1992), and Ogala (2011), the Cretaceous-Tertiary Anambra sediments contain coal reserves of different ranks occurring within formations. In the Lower Benue Trough, lignite and sub-bituminous coals occur within the Mamu and Nsukka Formations (Middle Campanian–Late Maastrichtian). These two distinct formations (called the Lower Coal Measures and the Upper Coal Measures) are separated by a great thickness of sandstone (Ajali sandstone) (Tattam, 1944). Lignite deposits occur in the Oligocene-Miocene Ogwashi-Asaba Formation. The Middle Benue Trough contains high-volatile bituminous coals found within the Awgu Formation (Middle Turonian–Early Santonian). The Upper Benue Trough contains lignites and sub-bituminous coals occur in the Gombe Sandstone Formation (Early Campanian–Late Maastrichtian) (Felix &Yomi, 2013). Together, the coal and lignite resource potentials are estimated at 1.5 billion tons and 300 million tons respectively.

However, the discovery of oil at Oloibiri in Bayelsa State in 1956 and the total dependence on oil and oil-derived foreign exchange in planning the nation's economy resulted in a steady decline of coal production and complete neglect of the coal industry with all its great economic potentials in the last few decades (Nwaobi, 2012; Odesola *et al.*, 2013). But, with increasing demand for more sustainable energy resources to meet economic growth and national development, the revitalization and further development of the coal industry regardless of the issues of acid mine drainage (AMD), infrastructural challenges, and lack of current geophysical data in coal sector can meet the energy demands of Nigeria's growing population (Ibitoye & Adenikinju, 2007; C.I.A.B., 2008; Board, 2009; World Coal Institute, 2009; Oguejiofor, 2010; Akujor *et al*., 2011; Board, 2012; Ohimain, 2014; Chukwu *et al*., 2016).

Geologically, Coal occurs in strata and exhibits significantly different petrophysical parameters in comparison to its surrounding rocks typically found in sedimentary basins (Hatherly, 2013), and requires advanced prospecting to provide necessary data for its exploration. Different techniques ranging from geological, geochemical, geophysical to drilling are been employed to evaluate coal deposits. However, its electrical properties have been suggested to be important for proper characterization during mining (Tiwary, 1993). The geophysical technique is very useful in many areas of environmental studies and conventional geotechnical testing as it uses non-invasive, cost-effective methods to probe the Earth (Anderson, *et al*., 2008; Arjwech *et al.*, 2013; Arjwech & Everett, 2015). In Coal investigation, it is advantageous before coal mining begins (Lei, 2015).

Geophysics applies the principles of physics to study the Earth (Kearey *et al.,* 2002) by detecting and analyzing variation in physical properties that are response to anomalous

bodies in the Earth. Measurements are done from above or below the Earth's surface at aerial, orbital, or marine platforms with comprehensive areal coverage at reduced prospection work time using a great variety of non-destructive sensing instruments. Different geophysical methods ranging from gravity, magnetics, seismic, resistivity, ground-penetrating radar, radiometric to electromagnetic are distinctively sensitive to contrasts in physical properties in the subsurface (Chalikakis *et al.*, 2011). However, the most informative data of the subsurface can be obtained following a combination of these methods. The results of geophysical exploration when combined with borehole data provide reliable data for future prospecting.

Of these methods, the resistivity method was employed for this research. The reason for the choice of this survey method is that rock materials show wide variation in resistance to electrical current flow and such contrast forms the basis for the application of the electrical resistivity method in coal exploration. Accordingly, the Electrical Resistivity Imaging (ERI) technique with a multi-electrode system was adopted to obtain imagery of the subsurface as most geological structures are not one-dimensional (1D). This technique has proven effective when routinely used in environmental engineering under a variety of field conditions and geological settings (Dahlin, 2001; Tselentis & Paraskevopoulos, 2002; Beresnev *et al.*, 2002; Godio & Naldi, 2003; Vickery & Hobbs, 2000; Wu, *et al*., 2016; Nwafor *et al.*, 2017). Some studies (Ewing *et al.*, 1936; Verma & Bhuin, 1979 and Singh *et al*., 2004), have confirmed that the electrical resistivity imaging (ERI) survey methods respectively can successfully be used to study coal deposits. Ewing *et al.*, (1936) revealed coal to have high resistivity to the surrounding formation when detected from borehole logs and DC resistivity surveying. Verma & Bhuin, (1979) and Singh *et al*., (2004), in their

report, confirmed this proposition using 1D and 2D electrical resistivity methods respectively for coal investigation.

1.2 Statement of the Problem

Coal occurs in strata with surrounding rocks and is explored and mined through scientific approaches. However, the search for Coal at an old mine working in Odagbo village is being carried out by artisan miners. These miners indiscriminately dig underground tunnels in search of Coal (see Plate I).This approach is imprecise, laborious, and harmful to miners and may create geohazards that affect the community and potential coal resources. These prompted the need for geophysical research, to obtain coal's subsurface data for mining within the area.

Plate I: Old mine workings (Left) and artisanal mining activities (Right) in Odagbo Area.

1.3 Justification of the Study

The increased demand for energy to meet the energy crisis in Nigeria has resulted in the search for more sustainable energy sources. Coal is one of the most important minerals in Nigeria that offer a major energy mix for electric power generation and feedstock for chemicals, fuels, and steel production for a developing country (see Plate II). It is a strategic resource that is widely attractive because of its abundance in many countries of the

world. Hence, the need for the development of Coal resources following proper exploration methods to meet sustainable development and attain the world standard.

To the best of my knowledge, no published work on geophysical research has been carried out in the study area. This geophysical research will provide vital information on coal resources that may serve as an incentive to potential investors and future researchers on coal in the area.

Plate II: Excavation of coal by Dangote Company in Unupi village (Left) and by artisan miners in Odagbo Area (Right).

1.4 Aim and Objectives

The aim of this research was to characterize Coal bearing layer at Odagbo Village, Kogi State, Nigeria using electrical resistivity imaging method.

The objectives of this research were to;

i. generate subsurface geoelectric sections of the study area,
ii. estimate the range of resistivity values associated with the subsurface rich in Coal seam,
iii. estimate the depth to the subsurface layer that is rich in the Coal seam, and

1.5 Location of the Study

Odagbo is a rural settlement in Ojoku district towards the northeastern part of Ankpa Local Government Area of Kogi State.It lies between latitudes 7º 28´ 30´´ N and 7º 29´ 00´´ N and longitudes 7º 43´ 30´´ E and 7º 44´ 0´´ E (see Figure 1.1).

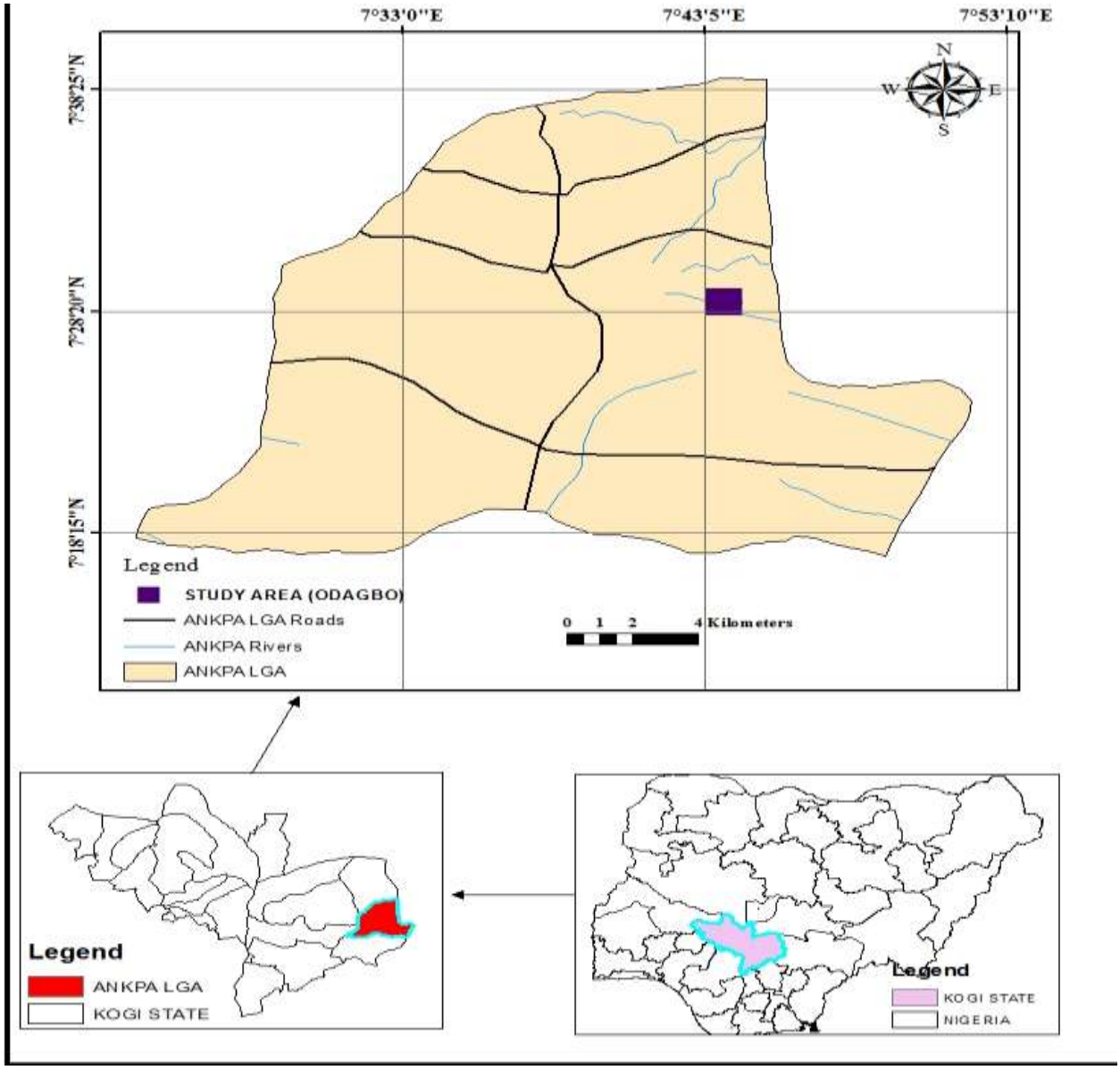

Figure 1.1: Location map showing the Study Area and its environs.

1.6 Geology of the Study Area

Odagbo is underlain by two geological formations, the Mamu Formation (coal-bearing) and Ajali Formation which form part of the Anambra Basin (Umeji, 2005) (see figure 1.2). The Anambra Basin is one of the intracratonic basins in Nigeria resulting from the deformation of the major depositional axis of the Benue Trough (Murat, 1972; Weber & Daukoru, 1975; Benkhelil, 1987). It is located in the southeastern part of Nigeria and lies between longitudes 6.30E and 8.00E, and latitudes 5.00 N and 8.00 N. It trends NE - SW obliquely across Nigeria with origin linked to the tectonic processes of separation of the African and South American plates in the Early Cretaceous (Murat 1972; Burke *et* al., 1972). It is bounded in the west by the Okitipupa Ridge, in the south by the Niger Delta Basin, to the northwest, it directly overlies the Basement Complex and interfingers with the Bida Basin. The basin is delimited in the north by the Basement Complex, the Middle Benue Trough, and the Abakaliki Anticlinorium. The basin covered an area of about 40,000 square kilometers with sediment thickness increasing southwards to a maximum thickness of 12,000 m in the central part of the Niger Delta. The sedimentary rocks are a Cretaceous depo-center that received Campanian to Tertiary sediments (Short & Stauble, 1967; Murat, 1972; Weber & Daukoru, 1975; Benkhelil, 1989; Nwajide, 1990; Obi *et al.*, 2001; Nfor *et al.*, 2005) such that strongly folded Albian-Coniacian succession (Pre-Santonian sediments) is overlain by nearly flat-lying Campanian-Eocene succession. It has enormous lithologic heterogeneity in both lateral and vertical extension (Agagu & Adighije, 1983; Akande *et al*., 2007; Akinyemi *et al.,* 2013).

The sequence of depositional events suggests a progressive deepening of the basin from the lower coastal plain and shoreline deltas to the shoreline and shallow marine deposits

(Adeleye, 1989; Anyanwu &Arua 1990; Fayose &Ola 1990; Akande & Mocke 1993; Adetona& Abu, 2013). This resulting succession comprises the Nkporo Group, Mamu Formation, Ajali Sandstone, Nsukka Formation, Imo Formation, and Ameki Group. Detailed stratigraphic description of these formations has been reported (Petters 1982; Agagu *et al.*, 1985; Reijers 1996). However, the Asu-River Group is the oldest facies (in the basin) dated Albian to Lower Cenomanian. This is overlain by Eze-Aku Formation dated Upper Cenomanian to Turonian age; further overlain by the pre-Santonian sediment deposit referred to as Awgu Formation dated Coniacian in age (Ola-Buraimo, 2013). Nkporo Group is overlain by Mamu Formation. It was deposited in Early Maastrichtian and comprises a succession of siltstone, shale, coal seam, and sandstone (Kogbe, 1976& Obi, 2004). The Mamu Formation (Lower coal measures) consists of siltstones, mudstones, grey carbonaceous shales, sandstones, and coal seams at several horizons (Ameh, 2013). The shales and mudstones are alternated with thin bands of siltstones. The rich coal deposits of Middle – Early Maastrichtian ages suggest brackish marshes during their deposition (Ogala *et al* 2012). Ajali sandstone (Maastrichtian) overlies Mamu Formation (Reyment, 1965 & Nwajide, 1990) which is mainly unconsolidated coarse-fine grained, poorly cemented; mudstone and siltstone (Kogbe, 1976). Ajali Sandstone is overlain by the diachronous Nsukka Formation (Maastrichtian-Danian) which is also known as the Upper Coal Measure (Reyment, 1965). Imo Shale (Paleocene) overlies Nsukka Formation (Nwajide, 1990). It comprises clayey shale with occasional ironstone and thin sandstone in which carbonized plant remains may occur (Kogbe, 1976). The Eocene stage was characterized by the regressive phase that led to the deposition of the Ameki Group.

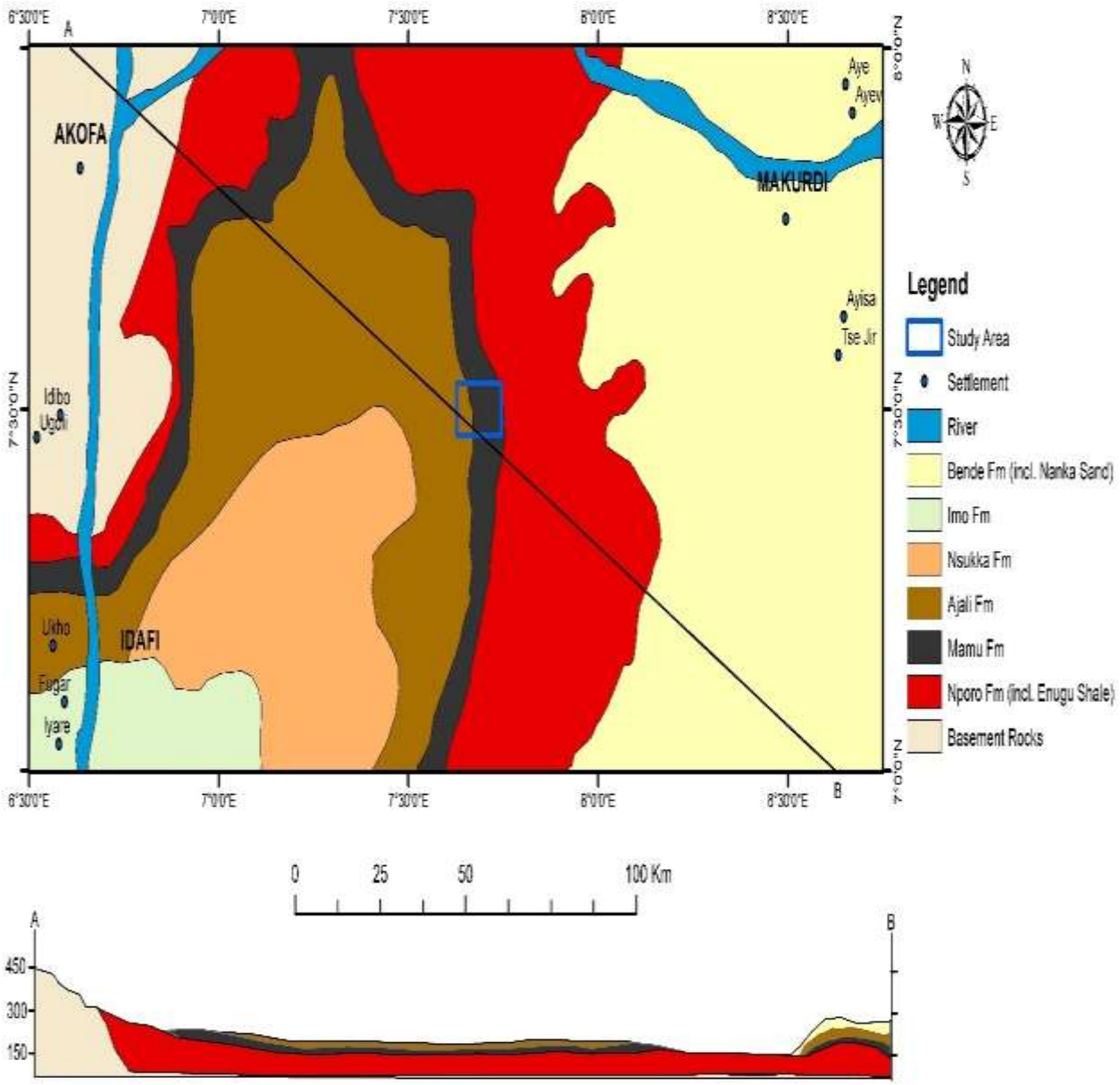

Figure 1.2: Geological Map of Anambra Basin Showing Study Area modified from (Bankole, *et al*., 2016).

CHAPTER TWO

LITERATURE REVIEW

2.1 The Coal Industry

Coal is a sedimentary rock, formed from the accumulation of altered dead plant remains-macerals, minerals, and water that became lithified at burial depth (see figure 2.1). Coal deposits are characteristic of thick non-marine sedimentary basins that have dominated certain areas of the world at different times in the past (Van Krevelen, 1957; Francis, 1961; Gluskoter, 1975; Taylor *et al.*, 1989; Speight, 2012; Speight, 2015).

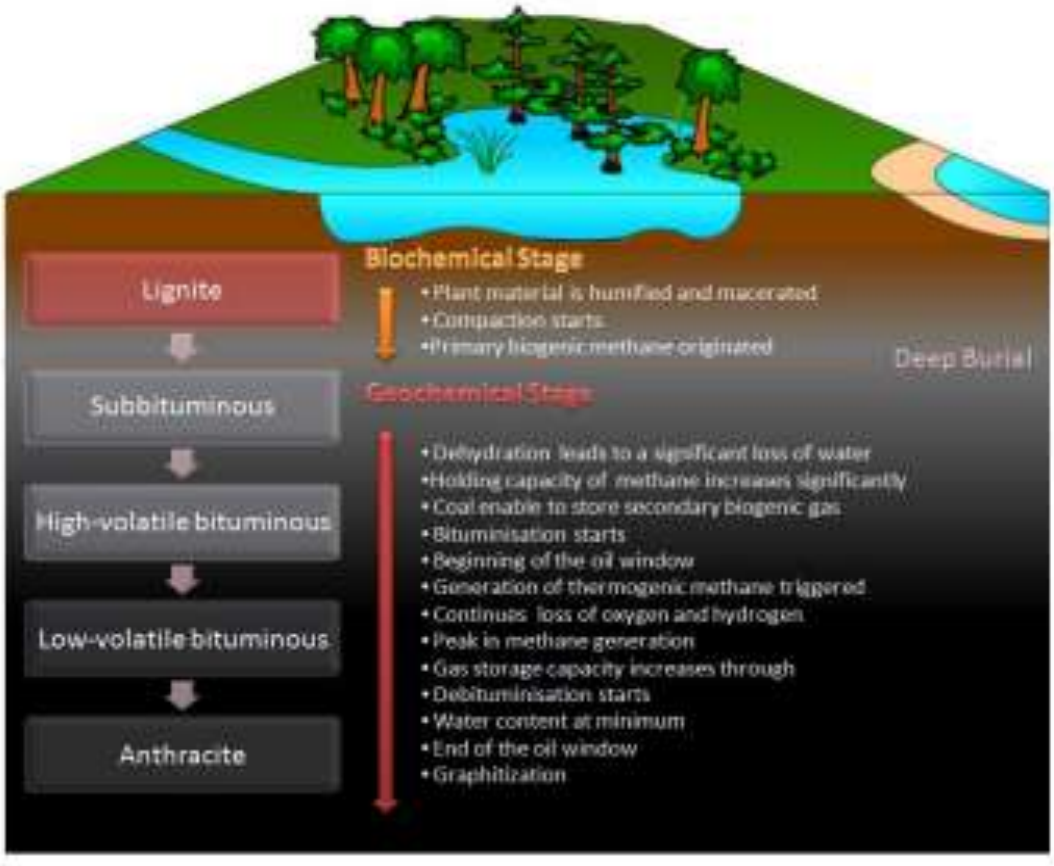

Figure 2.1: Coalification stages during coal generation (Langenberg, *et al.*, 1990).

The continuous transformation of plant material from peat to coal (known as coalification) is a process that can be divided into biochemical and geochemical stages. During the biochemical stage: biogenesis (the early stages of coalification), low drainage rate, and lack of freshwater help to create an acidic, low oxygen environment suited to anaerobic microbial communities that minimise decomposition and aid the accumulation of carbonaceous material. With the continued deposition of overlying inorganic sediments, this stage ends at depths of several hundred metres, where percolating water supplying microorganisms with nutrients is no longer available (Kim, 1978). The degree of maturation is referred to as coal rank, and at this point, coal can be already classified as lignite up to sub-bituminous (Langenberg *et al.*, 1990). Gradually, coalification enters the geochemical stage, where the sediment undergoes diagenesis driven chiefly by temperature (thermogenesis) and to a lesser extent pressure (Rightmire, 1984). With increasing depth, the plant materials are transformed by releasing volatile matter (water, carbon dioxide, and light hydrocarbons) and become progressively enriched in carbon and structurally more homogenous (Kim,1978; Langenberg *et al.*, 1990; Teichmüller & Teichmüller, 1968). In completion of the coalification range, the coal reaches the highest rank and is classified as a meta-anthracite.

Hence, the period of heating and pressure at burial depth, amounts of carbon content, and the amount of heat energy it can produce classifies coal into four main types or ranks (lignite, sub-bituminous, bituminous, anthracite). Lignite (brown coal) is the lowest rank of coal with 25-35% carbon and 45-60% moisture that makes up the lowest energy content between 4,000 and 8,000 Btu per pound. Lignite is mainly burned at power plants to generate electricity. Sub-bituminous coal is black in color and has a higher heating value

than lignite as it only contains about 35-45% carbon, and its moisture content lowers its heating value to between 8,000 and 13,000 Btu per pound. This coal is found very near to the surface, which makes its lower values. Bituminous coal appears shiny and smooth and has layers as it is formed when sub-bituminous coal is subjected to increased levels of organic metamorphism (i.e. under high heat and pressure). It contains 45-86% carbon and has two to three times the heating value of lignite. It is used to generate electricity and is an important fuel and raw material for the steel and iron industries. Anthracite is the highest grade of coal that has the highest heating value containing between 86-98% carbon and a moisture content of 15-20%. When it is burned, it produces very little ash and pollutants other than carbon dioxide. It is hard and brittle it experiences high temperatures and pressure during its existence, which points to most of it being found very deep in the earth (Kim, 1978).

Coal formation is a dynamic process with a great variety of factors involved, as such, there is no single molecular structure to represent a coal molecule; its heterogeneity in structure and composition is too great. But for simplicity, is a structure formed by clusters of weakly linked aromatic rings that break thermally during coalification to realign liberating volatiles (CO_2, CH_4, and H_2O) and hydrocarbon in a continuous process (Kim, 1977).

Coal is extracted from a deposit following several distinct steps from prospecting, analysis of the profit potential of the mine, mining of coal to final reclamation of the land after the mine is closed. The prospecting involves investigations undertaken on coal using geological sciences, geophysical, geochemical, and drilling technologies for future demand. However, the geophysical method has played a key role in coal seam mapping to estimate its resources and its economic potential before mining operations. This is followed by an

analysis of the deposit to evaluate its financial viability to inform the mining company whether or not to develop the mine. If approved, then coal is mined *in situ* using mining equipment such as dragline, electric or hydraulic shovels, or bucketwheel excavators. Two modern mining methods are usually employed; Opencast/surface mining and Deep/underground mining (Gluskoter, 1975; Vorres, 1993; Hartman, 2002;Ward, 2003).

Raw coal is then processed through a preparation plant (e.g., oscillating column) to remove contained impurities (e.g. rock, ash, sulfur) to improve its value before utilization. The process involves the crushing, screening into different sizes, separation by physical and chemical processes to remove undesired impurities (e.g., water, ash, Sulphur), and briquetting for the intended use. Commercial uses of coal by type including as fuel feedstock for industrial processes such as electricity generation, steel production, cement manufacturing, and domestic consumption (see figure 2.2). The properties that determine the economic viability and end-use category of coal are its rank (degree of coalification), chemistry, and physical properties.

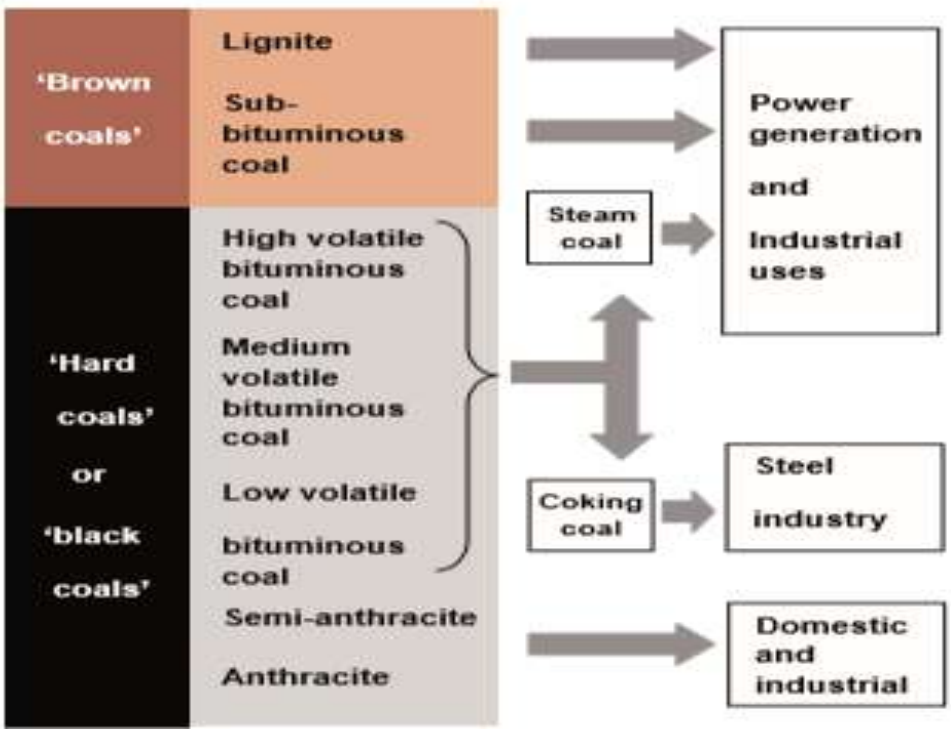

Figure 2.2: Coal specification and uses (Courtesy, www.UKMinerals.com)

However, Coal mining operations usually can destroy nature, pollute water, displaces settlers from their homes, and force the relocation of entire villages (Obiadi *et al.*, 2016; Momoh *et al.*, 2017; Adigun& Kayode, 2019). Clean Coal Technologies must be used by countries that rely on coal for its various uses to reach climate targets (Sambo, 2010, Fatoye & Gideon, 2013; Omoju, 2015). Alternative or clean coal technologies are used to reduce the environmental impact of coal by increasing the efficiency of its energy conversion and by reducing harmful emissions, notably of carbon dioxide and sulphur dioxide (Meduni, *etal*., 2018). Some of these clean coal technologies include chemically washing of minerals and impurities from the coal, gasification, carbon capture and storage (CCS), circulating fluidized bed combustion (CFBC), pressurized fluidized bed combustion (PFBC), Integrated Gasification Combined Cycle (IGCC) and top cycle ((Essien & Igweonu, 2014; Çelik, 2019; Edwards, 2019).

2.2 Previous Work

There is no record of any geophysical survey carried out in the present study area. However, a review of past works that are pertinent to this research is emphasized.

Sheets, (2002) carried out a survey in Ohio, United States using the electrical resistivity method in a bid to identify areas where coal was mined, distinguishing the areas from the air or water-filled voids. Several highly resistive areas were identified using dipole-dipole and Wenner resistivity surveys and subsequent drilling and excavation led to the discovery of several air-filled abandoned underground mine tunnels. After the high-resistivity response of air-filled voids within the sequence of coal-bearing rocks, electrical resistivity surveys can be a very effective tool for locating underground mine voids.

Johnson *et al.*, (2003) carried out an electrical resistivity survey to detect underground coal mine voids with the pole-pole configuration of 20 m electrode spacing in Lexington/Kentucky, United States. The authors concluded that results did not depict any relationship to the coal seam, but that the highest resistivity was immediately above the anticipated coal pillar.

Dahlin & Zhou, (2004) carried out a numerical modelling study with 10 electrode arrays to investigated their resolution capacity and efficiency. The result obtained show that the dipole-dipole, pole-dipole, and gradient arrays have the best resolution. But these arrays are most sensitive to noise as compared to the oftenused Wenner and gamma arrays. Considering the sensitivity to noise, they recommend the gradient, pole-dipole, and dipole-dipole arrays as well as Schlumberger array for 2D resistivity surveying requiring a high data density, because of their resolution capacity.

Singh *et al.,* (2004) used multielectrode resistivity imaging technique with pole-dipole electrode configuration to study coal seam located in the northern part of Jharia Coalfield of Dhanbad district, India. The obtained result gave electrical imaging of the subsurface as high-resolution pseudo-sections with coal seam having a high resistivity range of 989 Ωm to 1632 Ωm at depths varying between 10 m to 31 m from the surface.

Oladapo *et al.,* (2008) adopted the electrical resistivity method with Schlumberger electrodes configuration for the geoelectric study of coal deposits at the Unwana/Afikpo Area of Southeastern Nigeria**.** The authors reported that coal seams in Unwana have high resistivity characteristics contained within conductive host rocks. The coal seams were more intricate having shallow geoelectric attributes zones of thickness between 0.5 m to 1.9 m and overburden varying from 1.4 m to 7.9 m, moderately deep geoelectric attributes of thickness between 1.1 m to 7.7 m, and overburden varying from 7.4 m to 27.9 m are situated within the northeastern, south-central and southern parts of the study area.

Krishnamurthy *et al.,* (2009) employed electrical resistivity imaging technique to delineate coal seam barrier thickness and demarcate water-filled voids in an underground coal mine near Dhanbad, part of Jharia coalfield in India. The Mise-à-la-masse technique was used to establish a connection between water-logged areas and old mine workings. A good relation occurred between water-bearing zone(s) and coal pillars, and a high resistive zone ranging from 600 Ωm to 1000 Ωm below shallow depth was reported.

Ehinola *et al.,* (2012) employed Vertical Electrical resistivity Soundings (VES) to identify the areal extent of the coal and evaluate the coal thickness in Ute Area, particularly Ute and Okeluse towns, Southwestern Nigeria for domestic energy supplies for Nigeria. The authors identified four geoelectric layers, which include: the lateritic topsoil, shale, siltstone, and

coal horizon that has 1.02 x 107 tonnes reserve volume of coal for an area of 6.303 x 106 m^2 which may be commercially viable considering its area extent and must be exploited towards the northwestern part of Ute area.

Utom, (2012) used the resistivity method adopting the Schlumberger array to investigate the water quality, predict aquifer parameters, and acid mine drainage at Okpara coal mine, Enugu. In his findings, coal seams resistivity ranged between 1326 Ωm to 5831 Ωm at 3.1 m to 28.3 m. The aquifer is probably shallow with resistivity 28 Ωm to 527 Ω.m and thickness 2.1 m to 22.5 m.

Fatoye *et al.,* (2012) carried out a quality assessment on Cretaceous Okaba Coal in Anambra Basin, Nigeria to determine its quality for industrial usages. The authors reported from the result obtained that Okaba coal, is non-cokable and not suitable for use in the generation of heat for the working of blast furnace, but suitable for electric power generation and as a domestic fuel. Also, it is rich in resinous and waxy materials, as such, a suitable raw material for the chemical industry and in the manufacture of plastics, when fractionally distilled.

Aweto & Adaikpoh, (2014) used the electrical resistivity method adopting the square array method in a bid to delineate the geologic sequence at the Ezimo coalfield, as the square array method which was initially developed as an alternative to Wenner or Schlumberger array, can resolve dipping subsurface, bedding or foliation by isolating current direction. From their result, coal seam resistivity values ranged from 4900 Ωm to 9059 Ωm, and borehole records gave coal seam thicknesses ranging from 0.1 m to 2 m at the coalfields.

Chukwu *et al.,* (2016) characterized five coal samples from three different states in Nigerian; Odagbo (Kogi State), Owukpa (Benue State), Ezimo (Enugu State), Amansiodo

(Enugu State), and Inyi (Enugu State) to determine their suitability for power generation. The result classified them in terms of rank, grade, and type, and the ease of combustion of the coal samples in decreasing order is Odagbo < Owukpa < Inyi < Ezimo < Amansiodo.

Mohammed *et al.,* (2016) used the 2-D electrical resistivity method utilizing Wenner-Schlumberger array protocol to delineate the strike direction of coal deposit over part of Tai area of Gombe, northeastern Nigeria. The authors revealed two profiles taken in Northeast-Southwest (NE-SW) direction showing a clearer picture of the suspected coal seam because it was laid perpendicular to the strike direction and the other two profiles taken in Northwest- Southeast (NW-SE) direction was not pronounced because the profile was laid along the strike direction. Hence, the authors concluded the continuity of coal seams striking in the NW-SE direction and suggested for any future research profiles should be laid in the Northwest-Southeast direction to obtain an optimum result.

Momoh *et al.,* (2017) used Atomic Absorption Spectroscopy (AAS) to assess the concentration of trace elements in acid mine drainage (AMD) from Odagbo coal mine, North-Central, Nigeria. Comparisons were made between the trace elements and environmentally acceptable quality standard (EQS) for heavy metal discharges from mines using the student's *t-test*. The authors proposed no significant differences between the means of nickel, chromium, iron, and EQS for heavy metal discharges from mines ($P > 0.05$), while cobalt, iron, nickel, and chromium were the dominant trace elements in the AMD and suggested further studies are required to determine the influence of AMD on surface water and soils around the mine.

2.3 Resistivity Imaging

The basic principle for the successful application of geoelectric methods is based on the assumption that subsurface geological materials exhibit a wide variability of resistivity values to physical conditions such as lithology, porosity, the degree of water saturation, and the presence or absence of voids in the rock (Kneisel *et al.*, 2014). To determine the subsurface resistivity distribution, an artificially generated electric current is driven into the ground. In the assumption that the subsurface is continuous, a medium with conductive anomalies will have the current flow lines concentrate towards itself, while in a medium with resistive anomalies the current lines deviate around them, as seen in figure 2.3.

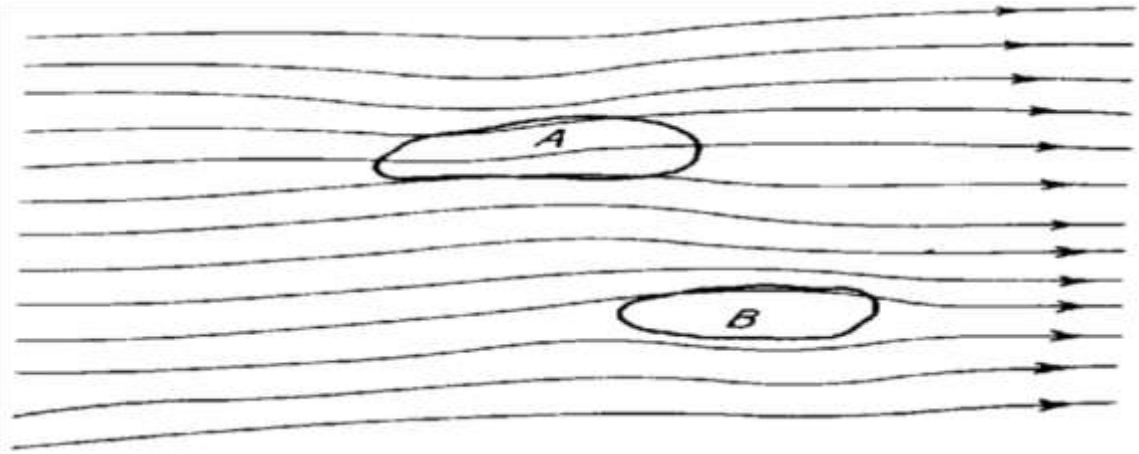

Figure 2.3: Distortion of current flow lines in (A) high and (B) low conductive anomaly (Jones *et al*., 2014).

The current flow patterns are altered following any variation in subsurface resistivity (conductivity) of earth materials, which in turn affect the distribution of electric potential. Placing two electrodes in the ground at a distance from each other and sending current between them causes an electrical field to spread into the earth around them. The electrical field penetrates more deeply into the subsurface when the current electrodes are farthest from each other, rather than when they are relatively close together. Thus, the potential of the field decreases with distance from the electrodes and its maximum on a line between

them (see figure 2.4). The resulting potential differences established, (P1 and P2) between two electrodes within that induced field are measured at the surface as deviations from the uniform earth representing the geological target of resistivity exploration. Multiplying the resistance by a geometric constant derived from the relative positions of the current and potential electrodes yields the resistivity of the material beneath the electrodes (Telford *et al*., 1990).

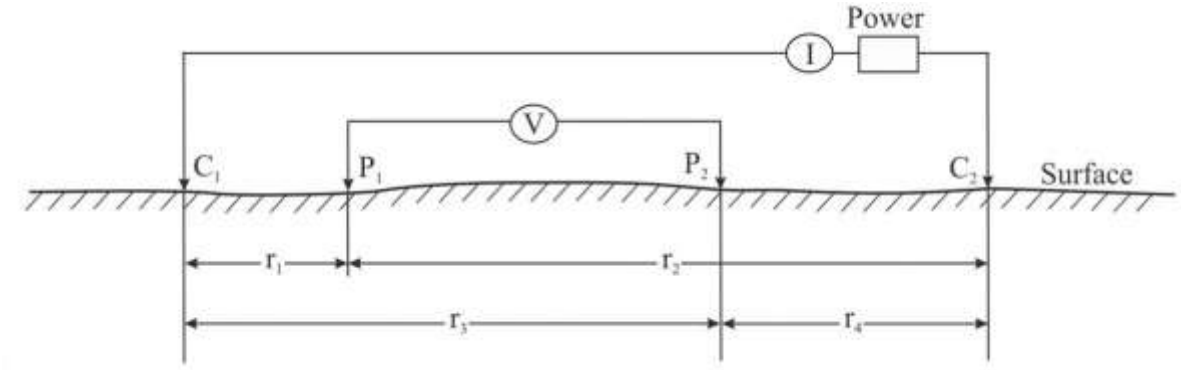

Figure 2.4: General four-electrode configuration with Current (C1, C2) and Potential (P1, P2) Distributions within Homogeneous Isotropic ground (Telford et al., 1990; Arjwech & Everett, 2015).

It is important to have dense enough data to cover laterally and in terms of the electrode, separations to recover in-situ bulk properties of complex structures in the ground. The advent of automated multi-electrode resistivity systems has led to rapid and efficient data acquisition of resistivity measurements. The electrical resistivity imaging (tomography) (ERI) uses several electrodes attached to a resistivity system with a switching module that makes it possible to carry out 2D, 3D, and 4D imaging surveys with tremendously increased efficiency and productivity (Griffiths & Barker, 1993; Dahlin, 2001; Stummer & Maurer, 2001; Auken *et al.*, 2006; Batayneh, 2006; Anderson *et al.*, 2008; Aizebeokhai, 2010; Griffiths &King, 2013). The multi-electrode resistivity system (ERI), however, is based on using the principle of a four-electrode method and the adoption of multiplexing of

several electrodes. A computer-controlled switching module chooses four predefined electrodes for every single measurement, sends the current, and measures the potential drop from which the resistance can be calculated (Loke *et al.*, 2013). Using several various combinations of transmitting and receiving pairs of electrodes, 2D/3D resistivity images can be constructed using appropriate inversion software. Moreover, using the time-lapse 3D resistivity technique, 4D resistivity data can be obtained (Chambers *et al*., 2013). With these improvements on the traditional 1D resistivity sounding and profiling, features of different resistivity properties to those of the surrounding material may be located and characterized in terms of electrical resistivity, geometry, and depth of burial. An example of 2D data collection using 20 electrodes with a Wenner array (Loke *et al*., 2013), is shown in figure 2.5.

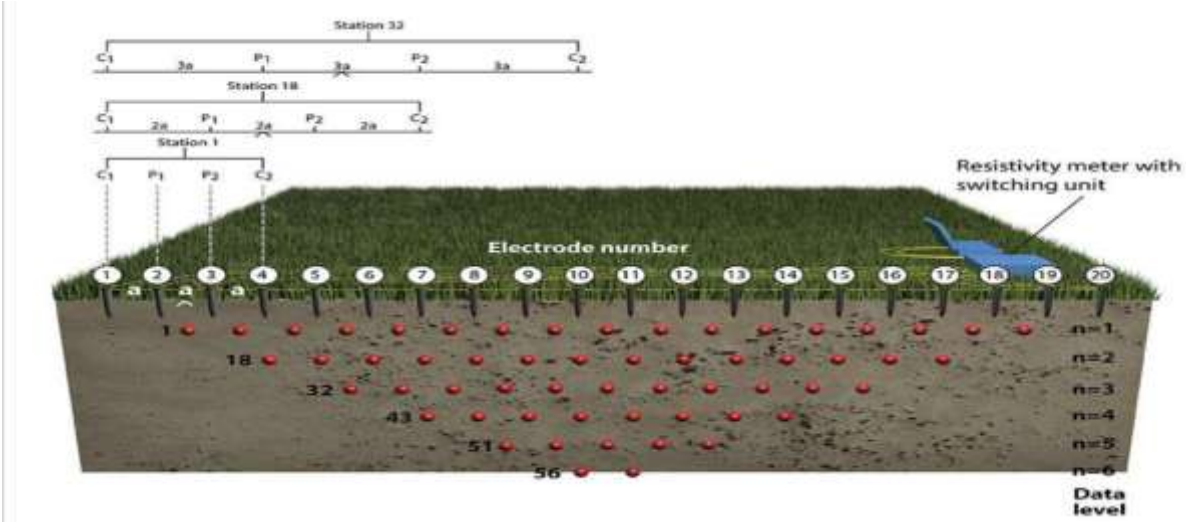

Figure 2.5: 2D data collection using multi-electrode resistivity system (Loke *et al*., 2013).

In the development of the 2D model, several (20) electrodes are installed along a line connected to the resistivity meter through multi-core cables. The measurements are progressively recorded for particular electrode spacing a (for Wenner array) and several acquisition levels (Griffiths & Barker, 1993). However, as the spatial distribution of

electrical properties is inherently 3D in nature, the 3D model can provide more accurate results, especially in environmental and engineering applications where the subsurface is highly complex (Aizebeokhai& Oyeyemi, 2014). In this mode, several electrodes are laid out in a square or rectangular grid with constant electrode spacing.

2.3.1 Theory of the Electrical Method

The resistivity method of geophysical prospecting is governed by Ohm's law which states that 'The electrical field strength at a point in a conducting material is proportional to the current density at that point (Ohm, 1827; Kirchhoff, 1857).

Mathematically, in vector form:

$$J=\sigma E \qquad (2.1)$$

where σ is the conductivity of the medium and E is the gradient of a scalar potential U (volts), i.e.

$$E=-\nabla U \qquad (2.2)$$

Putting equation (2.2) into equation (2.1)

$$J=-\sigma \nabla U \qquad (2.3)$$

From divergence condition,

$$\nabla . J = 0$$

Thus

$$\nabla . J = -\nabla . (\sigma \nabla U) = 0$$

Or,

$$\sigma \nabla . U + \sigma \nabla^2 U = 0 \qquad (2.4)$$

For a homogeneous earth, σ is a constant and since the derivative of a constant is equal to zero, then the first term in equation (2.4) vanishes hence,

$$\nabla^2 U=0 \qquad (2.5)$$

Equation (2.5) is called Laplace equation.

Applying boundary conditions, equation (2.5) can be solved for specific cases. For instance, for a single current electrode at the surface of a homogeneous ground, equation (2.5) is expressed in spherical polar coordinates as:

$$\frac{1}{r^2}\frac{\partial}{\partial r}\left(r^2\frac{\partial U}{\partial r}\right)+\frac{1}{r^2\sin\theta}\frac{\partial}{\partial\theta}\left(\sin\theta\frac{\partial U}{\partial\theta}\right)+\frac{1}{r^2 sin^2\theta}\left(\frac{\partial^2}{\partial\phi^2}\right)=0 \qquad (2.6)$$

For point current source, there is complete symmetry of current flow with respect to the **θ** and $\boldsymbol{\phi}$ directions and the derivatives with respect to these directions are zero. Thus, equation (2.6) becomes;

$$\frac{d}{dr}\left(r^2\frac{dU}{dr}\right)=0 \qquad (2.7a)$$

Integrating equation (2.7a) gives;

$$r^2\frac{du}{dr}=a$$

$$du=\frac{a}{r^2}dr$$

$$\int du=a\int\frac{dr}{r^2}$$

$$U=-\frac{a}{r}+b \qquad (2.7b)$$

Where **a** and **b** are constants, U is the electric potential at the measuring point and r is the distance from that point to the single current electrode. Since *U=0* as r→∞ then b = 0 and

$$U=-\frac{a}{r} \qquad (2.8)$$

The current flows radially outwards in all directions from the point current electrode and the total current crossing a sphere of radius **r** is;

$$I = 4\pi r^2 J$$

By applying equations (2.3) and (2.8).

$$I = -\frac{4\pi a}{\rho} \qquad (2.9)$$

Thus

$$a = -\frac{I\rho}{4\pi} \qquad (2.10)$$

Putting equation (2.10) into equation (2.8) we have;

$$U = \frac{I\rho}{4\pi}\frac{1}{r}$$

$$\rho = 4\pi r\left(\frac{U}{I}\right) \qquad (2.11)$$

The equipotential that is everywhere perpendicular to the current flow lines will be spherical surfaces given by **r** is equal to a constant.

The point current electrode of the three-point-system is located at the surface of the homogeneous isotropic medium with the air above having zero conductivity, the return current electrode is at a great distance. As in the previous case b=0 since U=0 as r→∞

In addition, $\frac{\partial U}{\partial Z} = 0$ at $z = 0$

Since $\sigma_{air} = 0$ In the present case, all the current flows through a hemispherical surface in the lower region.

Hence

$$U = \frac{I\rho}{2\pi}\frac{1}{r} \qquad (2.12)$$

For two-point current electrodes on the earth's surface, we apply equation (2.12) to the general four-electrode arrangement (Figure 2.4) to obtain potential difference ΔU, between potential electrodes P_1 and P_2. That is,

Given,

r_1 = C1 P1, r_2 = C2 P1, r_3 = C1 P2 and r_4 = C2 P2

As before, the potential due to C1 at P1 is

$U_1 = -\frac{a_1}{r_1}$ Where $a_1 = -\frac{I\rho}{2\pi}$

Similarly, the potential due to C2 at P1 is

$U_2 = -\frac{a_2}{r_2}$ Where $a_2 = \frac{I\rho}{2\pi}$

$a_2 = -a_1$, since the current at the two electrodes are equal and opposite in direction.

Therefore, the potential at P1 due to both current electrodes is,

$$U = U_1 + U_2 = -\frac{a_1}{r_1} - \frac{a_2}{r_2} \quad (2.13)$$

Substituting the expression of a_1 and a_2 into equation (2.13),

$$U = \frac{I\rho}{2\pi}\left(\frac{1}{r_1} - \frac{1}{r_2}\right) \quad (2.14)$$

Similarly, when the second potential electrode is introduced at P2, the potential at P2 due to both current electrodes is

$$U = \frac{I\rho}{2\pi}\left(\frac{1}{r_3} - \frac{1}{r_4}\right) \quad (2.15)$$

Then, the potential difference between P1 and P2 is,

$$\Delta U = \frac{I\rho}{2\pi}\left\{\left(\frac{1}{r_1} - \frac{1}{r_2}\right) - \left(\frac{1}{r_3} - \frac{1}{r_4}\right)\right\}$$

$$\Delta U = \frac{I\rho}{2\pi}\left[\frac{1}{r_1} - \frac{1}{r_2} - \frac{1}{r_3} + \frac{1}{r_4}\right] \qquad (2.16)$$

Such an arrangement corresponds to the four-electrode spread normally used in resistivity field work, where **ρ** is the resistivity, **I** is the current and r_1, r_2, r_3, and r_4, are the inter-electrode distances (Figure 2.4).

From equation (2.16), the resistivity can be solved as;

$$\rho = \frac{\Delta U}{I}\frac{2\pi}{\left[\frac{1}{r_1} - \frac{1}{r_2} - \frac{1}{r_3} + \frac{1}{r_4}\right]} \qquad (2.17)$$

Because of a non-homogeneous earth and the actual current flow is highly influenced by conductive layers, the value measured is known as the "apparent resistivity". In its simplest terms, the apparent resistivity represents an average value encompassing all of the different materials within the volume (half-space) of materials being measured (Milsom, 2003).

The apparent resistivity $\boldsymbol{\rho_a}$can therefore be represented as;

$$\rho_a = \frac{\Delta U}{I} K_f \quad (2.18)$$

where K_f is known as the geometric factor = $\frac{2\pi}{\left[\frac{1}{r_1} - \frac{1}{r_2} - \frac{1}{r_3} + \frac{1}{r_4}\right]}$

The result is independent of the position of the electrodes and is not affected when the current and the potential electrodes are interchanged.

Theoretically, the four electrodes can be placed at any arbitrary locations on the soil surface. However, a few electrodes arrays are popular and have been used for data acquisition (Szalia& Szarka, 2008). Each array has characteristic features that make it suitable for a particular application. Figure (2.6) shows a table of the popular electrode arrangements and the corresponding geometric factors: a is the electrode spacing and n is the spacing integer factor.

Array Type	Electrode Arrangement	Geometric Factor (K)
Wenner	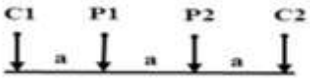	$2\pi a$
Schlumberger	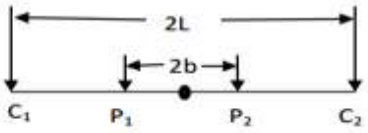	$\frac{\pi}{2}\left(\frac{L^2}{b}-\frac{b}{2}\right)$
Wenner-Schlumberger	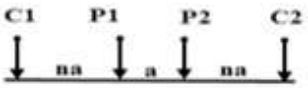	$\pi n(n+1)a$
Dipole-Dipole	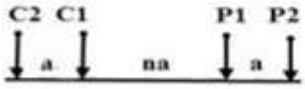	$\pi n(n+1)(n+2)a$
Square	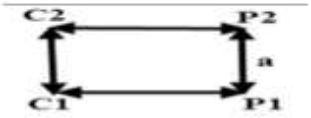	$2\pi a/2\sqrt{2}$

Figure 2.6: Popular electrode arrangements modified from Samouolian *et al*., (2005).

2.3.2 Electrical Resistivity of Earth Materials

Among all the physical properties of the earth materials (rocks and minerals), electrical resistivity shows the largest range of variations. Resistivity varies from about 10-8 Ωm, for native metallic minerals, to 1016 Ωm for pure Sulphur, between this limit lies other earth materials (Telford *et al*., 1990).

Several factors affect the resistivity of earth materials and can be classified as either been geologic or hydro-geologic in nature. Chiefly among the geologic factor is mineral composition. The common rock-forming minerals such as silicates, phosphates, carbonates,

nitrates, and so on are poor conductors. The variation in the resistivity of minerals is quite large. Figure (2.7) showsthe resistivities of common rocks and minerals.

Temperature, structure, and texture of rocks, and porosity also influence resistivity values. An increase in temperature lowers the viscosity of water, increased the mobility of the ions, and is observed as resistivity decrease. Well-sorted rocks have high resistivities while poorly sorted rocks have lower resistivities. Geological processes; dissolution, faulting, and shearing usually increase porosity and fluid permeability, and hence lower resistivity. Precipitation of calcium carbonate and silica reduces porosity and hence reduces fluid permeability and increases resistivity. Induration by compaction or metamorphism will reduce porosity and permeability and hence increases resistivity (Keller & Frischknecht, 1966).

Hydro-geologic factors such as water saturation and salinity affect the resistivity of sub-surface materials. Since the minerals which form the matrix of rocks are generally poorer conductors than the groundwater, the effective resistivity of the rock is decreased by the groundwater. Thus, any small change in the percentage of the water content affects the resistivities of the earth materials significantly. Electrolytic conduction from ions of dissolved salts in water in the pore spaces of rocks also tends to affect resistivity. The greater the amount of dissolved salt, the lower the resistivity and vice versa.

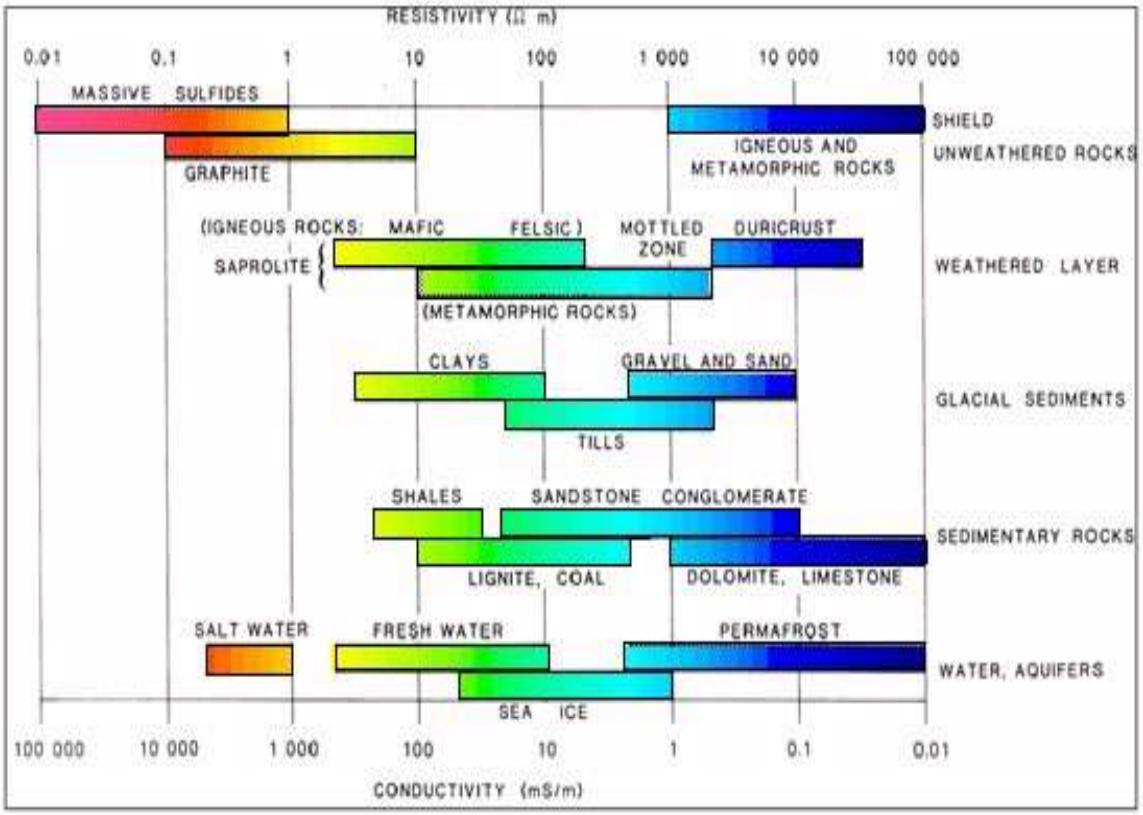

Figure 2.7: Resistivities of Rocks, Soils and Minerals adapted from Palacky, (1988).

Generally, igneous and metamorphic rocks typically have high resistivity values from above 1000 to 10 million Ωm, based on the degree of fracturing and the percentage of the fractures filled with groundwater. Sedimentary rocks, which are usually more porous, and have higher water content and salinity, normally have lower resistivity values from 10 to about 10000 Ωm, with most values below 1000 Ωm (Daniels & Alberty, 1966). Unconsolidated sediments also have even lower resistivity values ranging from about 10 to less than 1000 Ωm dependent on the porosity as well as the clay content. The resistivity of groundwater varies from 10 to 100 Ωm depending on the concentration of dissolved salts. This characteristic is useful in the detection of fracture zones and other weathering features, for engineering and groundwater surveys (Telford *et al*., 1990).

CHAPTER THREE

MATERIALS AND METHODS

3.1 Materials

The following materials were used for the study;

1. Global positioning system (GPS)
2. ABEM Lund imaging system (SAS 4000)
3. Cables and reels
4. Hammers
5. Measuring tape
6. UPS Battery and its charger
7. A computer
8. Software for processing and analyzing the geophysical data (SAS 4000 Utilities software, RES2DINV).

3.2 Methodology

3.2.1 Reconnaissance Survey

Reconnaissance surveys were carried out to obtain information about the study area. Firstly, by reviewing previous works in the study area and its environs. Then, visiting the study area to see how the terrain looks like and also see possible areas where Coal is suspected. Ground materials from old mine workings along with the present level of artisan activities were observed. G.P.S coordinates and photographic images were taken at strategic points, to mark areas in which profiles will be laid.

3.2.2 Instrumentation: The ABEM LUND Imaging System

The basic part of any resistivity measurement system includes a source of electrical current (either D.C or low-frequency A.C), a voltage measuring system, and the cables to connect these components to the electrodes. However, with growing interest for better field techniques, these components have undergone major modifications over the years to improve the efficiency of the survey procedure, the quality of the data, and to increase the depth of investigation. Hence, the development of computer-controlled data collection and automatic data inversion.

Automated multi-electrode resistivity systems use the principle of the traditional four-electrode method and multiplexing several electrodes. A typical computer-controlled system (Dahlin, 2000; Stacey, 2006; Damasceno *et al*., 2009; Sherrod *et al*., 2012) consists of three main parts (see figure 3.1): (1) data acquisition and control system; (2) electrode configuration and connection; and (3) a third-party reconstruction software. The system, however, must offer flexible control of the current and voltage readings, high-speed data acquisition, and appropriate computer interfacing (Tsourlos, 1995; Dahlin, 2001; Polydorides, 2002; Stummer *et al.*, 2002; Stacey, 2006; Damasceno *et al*., 2009). Such is the ABEM LUND Imaging System which was used for this survey.

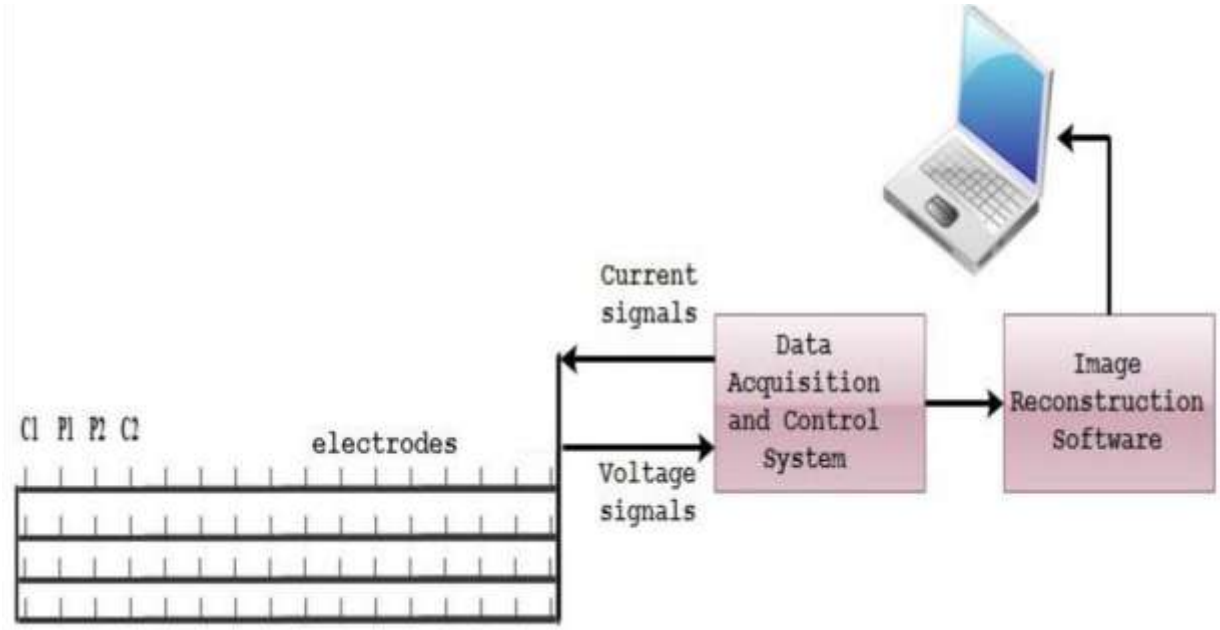

Figure 3.1: A Schematic diagram of an automated multi-electrode resistivity system (Stummer & Maurer, 2001).

The LUND Imaging system is a multi-electrode system for automatic resistivity profiling and drilling. It is cost-effective and suited for high-resolution 2D and 3D resistivity surveys. The LUND Resistivity Imaging System consists of a basic unit, a standard resistivity meter (ABEM Terrameter SAS (1000/4000)), and a (4x64) multi-channel relay matrix switch unit called Electrode Selector (ES) 464. The system also has four multi-conductor electrode cables wound on reels each having 21 take-outs, stainless steel electrodes, and cable jumpers, and various connectors. The system is compatible with a portable PC-type computer or Laptop. Its operating power comes from an internal 12 volts rechargeable NiCd battery pack. Model section plotting of 1D, 2D, and 3D model interpreted in colour or grayscale including topography reference data and reference levels, utility software for extraction of VES, data manipulation and conversion, graphical output in PCX-file format, *etc.*, are also available(ABEM, 2010).

The Lund ES 464 basic system used for this survey, consists of one ES 464 field unit with a clip-on NiCd rechargeable battery pack and one communication cable from electrode selector to Terrameter. It is lightweight and has a waterproof, rugged cast aluminum casing. The Terrameter SAS system consists of a basic unit called the Terrameter SAS 4000. It is a method whereby consecutive readings are taken automatically and the results are averaged continuously. Signal Averaging System (SAS) results are more reliable than those obtained from single-short systems. The SAS 4000 system can operate in different modes, e.g., resistivity, self-potential, and induced polarization. In all its modes it is capable of measuring simultaneously in four channels thus making it suitable in all sorts of resistivity surveys.

The SAS 4000 is powered by a clip-on NiCd battery pack that clips conveniently onto the bottom of the instrument or by an external 12 volts source. The SAS-EBA external 12 volts adapter allows the Terrameter to utilize an external 12 volts D.C. source e.g., a car battery. Stainless steel electrodes establish electric contact through long cables, to an ionic conductor which is the ground. All sorts of electrodes generate "noise". Noise is the fluctuating voltage that appears between a pair of electrodes placed so close that no other natural voltages appear. The problem of polarization can be tackled by periodically reversing the current electrode polarity (Tsourlos, 1995) or by using special nonpolarized electrodes (Samouëlian *et al.,* 2005); however, they are difficult to implement and expensive (Wilkinson *et al.,* 2012). But stainless-steel electrodes are less affected by polarization and create less noise than electrodes made of ordinary steel (LaBrecque & Daily, 2008). Practically, adopting special measurement sequences and considering an adequate time delay between using an electrode to inject current and to measure voltage can

significantly reduce the polarization effect (Dahlin, 2000; Winkinson *et al.*, 2012). An AC source at low frequency can be used to prevent an accumulation of ions so that electric polarization is minimized. However, electromagnetic effects have to be considered (Tsourlos, 1995).

Current electrodes and potential electrodes make good contact with the ground to ensure low contact resistance and stability respectively (ABEM, 2010). The current and potential electrodes in multi-electrode resistivity systems are switched through multiplexers. The switching mechanism should be reliable for any electrode arrangement (Loke *et al.*, 2011). The cables incorporate heavy gauge conductors with excellent insulation to ensure good survey results. The cables are expandable for deeper penetration by connecting them in series with cable joints. The cables have take-outs at 5m intervals along its length from which the cables are connected to the electrodes using cable jumpers having crocodile clips at both ends. Depending on the application, the electrode take-out spacing varies from less than 1 to 25 m or more (Dahlin, 2001). The cables are wound on reels (see plateIII).

Plate III: ABEM LUND Imaging System and accessories.

3.3 Choice of Array Configuration for the Survey

The Dipole-Dipole array configuration was used for the field survey. The dipole-dipole array is the most sensitive to resistivity variations below the electrodes in each dipole pair and is very sensitive to horizontal variations with depth. Thus, it is the most sensitive array to 3D structures among the common arrays and has low electromagnetic coupling between the current and potential circuits (Dahlin & Loke, 1997). Hence, the choice of this array was based on its sensitivity to 3D structures, most efficient in areas with great lateral variations in depth to bedrock and also good horizontal data coverage and as a result can be successfully used in the detection of coal (Zhou *et al.*, 2000; Dahlin & Zhou, 2004).

The arrangement of the electrodes is as shown in figure (3.2). The potential electrodes M and N are not placed between the current electrodes A and B. The dipole-dipole array is logically the most convenient array used in the field especially for a large-scale survey. In this type of array, all four electrodes are placed along the same line and the distance

between the current electrodes A and B is equal to the distance between the potential electrodes M and N represented by ‘a’. The distance between the middle points of current and the passive electrode sets is an integer multiple of ‘a’ and the factor itself is assigned to be equal to ‘n’.

The geometric factor K can be found from the following expression:

$$K = \pi n(n + 1)(n +2)a \quad (3.1)$$

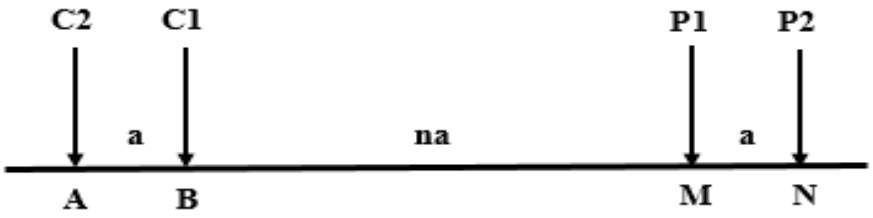

Figure 3.2: The dipole-dipole array configuration (Zhou *et al*., 2000).

3.4 Data Acquisition

The geophysical data acquisition was conducted between the 19th of April to 22th of April 2019 with the use of the ABEM SAS 4000 Terameter system and multi-core cable systems. The field measurement began with laying out of multi-core cables (reels) and electrodes along with the chosen profile while coordinates of the start, middle, and endpoints along the profile are recorded. Each cable has 21 electrode take-outs, spaced 5 m apart. The Terrameter SAS 4000 and the ES 464 were positioned at the center of the layout. The two cables were connected to the Electrode selector (ES 464) at the center of the layout. Take-out 1 and take-out 21 were made to overlap at the cable ends and the layout centre, and mid-point was determined by stacking the first electrode take-out of the second reel with the last electrode take-out of the first reel. The serial port of the Terrameter was connected to the electrode selector (through a communication cable) and the electrodes connected to all the take-outs at the intervals of 5 m on the reels using cable jumpers. The electrode take-

outs at the mid-point were connected to the positioned electrode at that point via two jumpers. The electrodes were hammered into the ground for dry and hard ground and hand-pushed where the ground is moist or soft. The Terrameter was then connected to an external 12 volts battery and switched on, which automatically switch on the Electrode Selector, and the system set-up displays on the screen. The Terrameter was set to resistivity mode and LUND Imaging, and measurement was carried out after the contact resistance test output gave a good result. The programmes automatically continue to measure apparent resistivity values (displayed on the screen) using the two electrode cables. When measurements on each layout were finished, the programne was stopped and the Terrameter was switched off, and the whole equipment is transferred to a new profile and the entire process repeated. Measurements were made along 9 profiles on two areas within the mining site; Area A (known mining site) and Area B (unexcavated site). Two profiles were taken at Area A in a dench and seven profiles at Area B in an elevation. At Area A, the first profile was located about 10 m away from the nearby open-pit mine and the second profile was 50 m away from the first profile. The choice of profile location was made in an attempt to obtain control for the result while minimizing the error that is caused by the presence of the nearby excavation. At Area B, the subsequent seven profiles were located about 50 m further away from the open-pit mine area. Five profiles were located 10 m away from each other, while the last two profiles were located perpendicular to the start and end of the five parallel profiles. The choice of direction of these profiles was for continuity of the coal to be mapped and to be able to get its depth and strike direction. Each cable covers 200 m between the first and the last take-out. A grid of 41x5 electrodes was covered for each survey profile. Figure (3.3) shows the profile's layout in the study area. Profile 1 is labelled P1 to P1′ and the subsequent profiles are in the same format. Table (3.1) is the record for

Coordinates startpoints, midpoints and endpoints for each profile. Also, Plate (IV) shows ERI data acquisition of profile 1 in the study area near the mining pit.

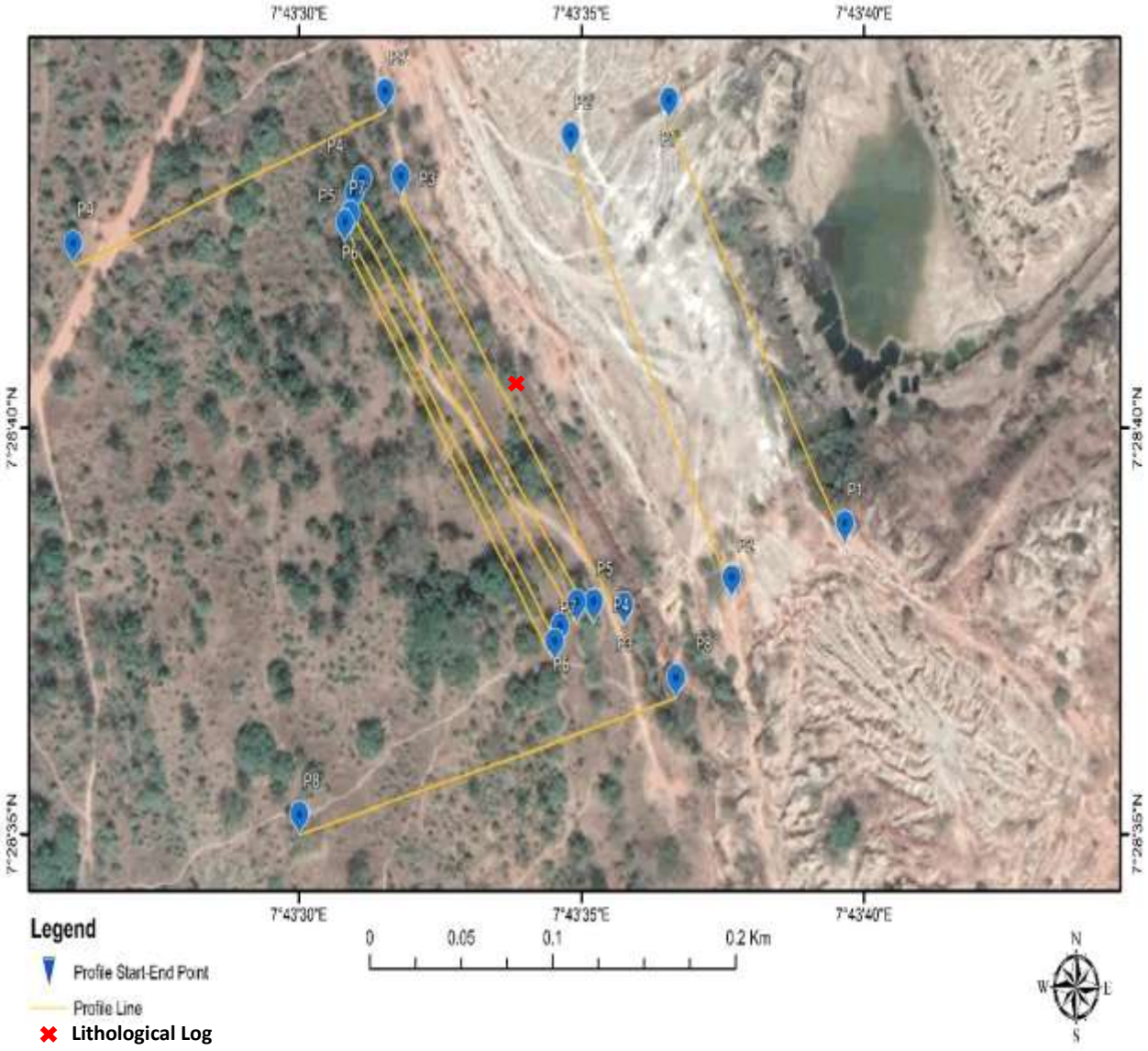

Figure 3.3: Google earth image illustrating the ERI layout in the study area (courtesy Google earth software).

Table 3.1: Coordinates of start points, midpoints and end points along the profiles.

S/N	Profile	Start Point	Mid-Point	End Point
1	1	N07^0 28′ 38.5″ E07^0 43′ 39.2″	N07^0 28′ 41.4″ E07^0 43′ 38.0″	N07^0 28′ 44.4″ E07^0 43′ 36.8″
2	2	N07^0 28′ 38.1″ E07^0 43′ 37.9″	N07^0 28′ 41.0″ E07^0 43′ 36.4″	N07^0 28′ 43.9″ E07^0 43′ 35.0″
3	3	N07^0 28′ 38.0″ E07^0 43′ 35.7″	N07^0 28′ 40.6″ E07^0 43′ 33.9″	N07^0 28′ 43.3″ E07^0 43′ 32.0″
4	4	N07^0 28′ 37.8″ E07^0 43′ 35.4″	N07^0 28′ 40.5″ E07^0 43′ 33.5″	N07^0 28′ 43.2″ E07^0 43′ 31.7″
5	5	N07^0 28′ 37.8″ E07^0 43′ 35.1″	N07^0 28′ 40.1″ E07^0 43′ 33.3″	N07^0 28′ 43.0″ E07^0 43′ 31.2″
6	6	N07^0 28′ 37.5″ E07^0 43′ 34.8″	N07^0 28′ 40.0″ E07^0 43′ 32.9″	N07^0 28′ 42.8″ E07^0 43′ 31.1″
7	7	N07^0 28′ 37.3″ E07^0 43′ 34.7″	N07^0 28′ 39.7″ E07^0 43′ 32.7″	N07^0 28′ 42.7″ E07^0 43′ 31.0″
8	8	N07^0 28′ 37.8″ E07^0 43′ 36.2″	N07^0 28′ 36.7″ E07^0 43′ 33.1″	N07^0 28′ 35.1″ E07^0 43′ 30.2″
9	9	N07^0 28′ 42.6″ E07^0 43′ 33.8″	N07^0 28′ 40.6″ E07^0 43′ 30.2″	N07^0 28′ 35.1″ E07^0 43′ 29.0″

Plate IV: ERI data acquisition in the study Area.

3.4.1 Field problems

Some of the problems encountered during the field measurement are as follows:

1. Draining of the battery during the field measurement slows down the measurement and the battery has to be recharged after some measurements were taken. eventually, an alternative battery had to be provided which increased the field survey expenses.

2. Sometimes poor contact existed between the electrodes and ground when the electrodes where hammered vertically into the ground. few drops of water and salt was applied at each affected electrode point to ensure good contact.

3. The practical difficulty in moving great length of cables and electrodes around was also very tasking. available manpower improvised on how to move equipment to ensure fast data acquisition.

3.5 Data Processing

In the data processing, series of steps were taken to remove spurious noise and/or signals from the obtained data for interpretation of the relevant signal. The measured apparent resistivity data files for all the resistivity imaging profiles were downloaded from the ABEM ES464 Terrameter into a computer (using a rewriteable compact disc) with installed ABEM file conversion (SAS4000 Utilities) and RES2DINV application software. The SAS4000 Utilities software was used to convert the original data file (in.s4k format) to the appropriate (.DAT format) input file readable by the inversion software (RES2DINV). A total of nine files were converted for processing using RES2DINV (Loke & Barker, 1996). However, these resistivity data sets were first inspected for the presence of unreasonably high and low (negative) resistivity values called "bad data points" (Loke, 2010). If any, such points were removed manually by simply clicking on them as illustrated in figure (3.4) before the compilation of a resistivity model/ERI resistivity profile that displays horizontal and vertical resistivity distribution (see figure 3.6).

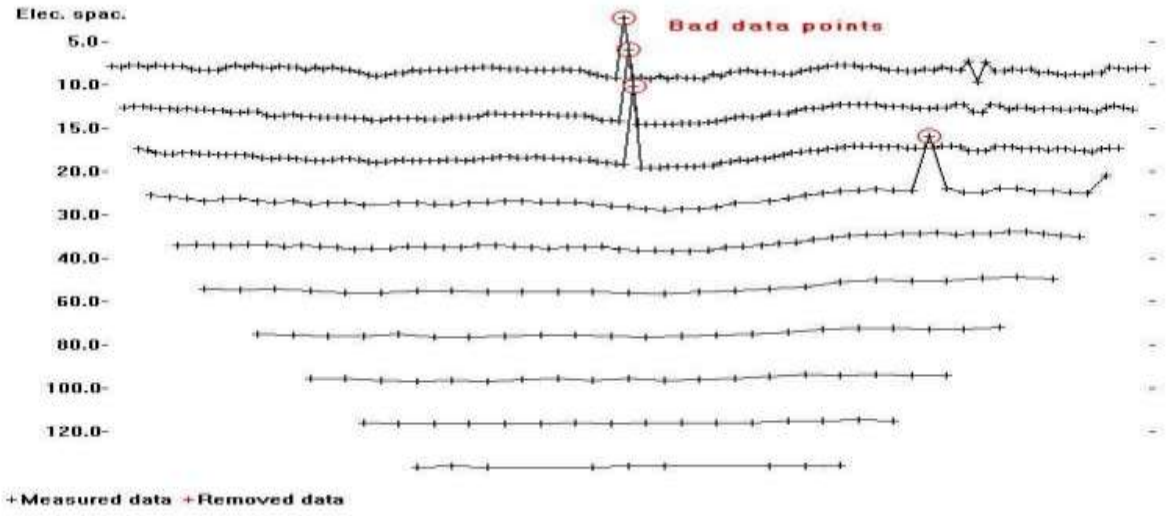

Figure 3.4: An example of a profile showing data set with a few bad data points. (Loke, 2010).

The RES2DINV application software is a computer programme that automatically creates a 2D resistivity model and IP model of the subsurface from an electrical survey using an inversion routine that divides the subsurface into rectangular blocks (Loke & Barker, 1996). Two inversion techniques are routinely used in resistivity data inversion, these are; the standard least-square smoothness constrains and robust constrain inversion techniques (see figure 3.5). The standard constrains inversion technique, also called the L2 norm was used. This method is based on the following equation:

$$(J^TJ + \lambda F)\Delta Q_K = J^Tg - \lambda F Q_K \quad (3.2)$$

where

$F = \alpha_x C_x^T C_x + \alpha_z C_z^T C_z$

C_x = Horizontal roughness filter

C_z = Vertical roughness filter

J = Jacobian matrix of partial derivatives

J^T = Transpose of J

λ = Damping factor

Q = Model change vector

g = Data misfit vector

C_x^T = Transpose of horizontal roughness filter

C_z^T = Transpose of vertical roughness filter

In this technique, the least-squares method reduces the square of the differences between the observed and the calculated apparent resistivity values. At the same time, it also attempts to reduce the squares of the changes in the model resistivity values (deGroot- Hedlin & Constable, 1990). This will give a subsurface model whose resistivity values will be smoothly varied. This type of model is suitable in an environment where

subsurface resistivity values are changing in a smooth manner (Loke *et al.*, 1999). This method can only produce reasonable results if the data contains random or "Gaussian" noise. If the data set however contains "outlier" data points (i.e., the noise that originates from non-random sources such as mistakes or equipment problems), the results obtained will be less satisfactory. This is because such "outlier" data points could have a great effect on the resulting inversion model.

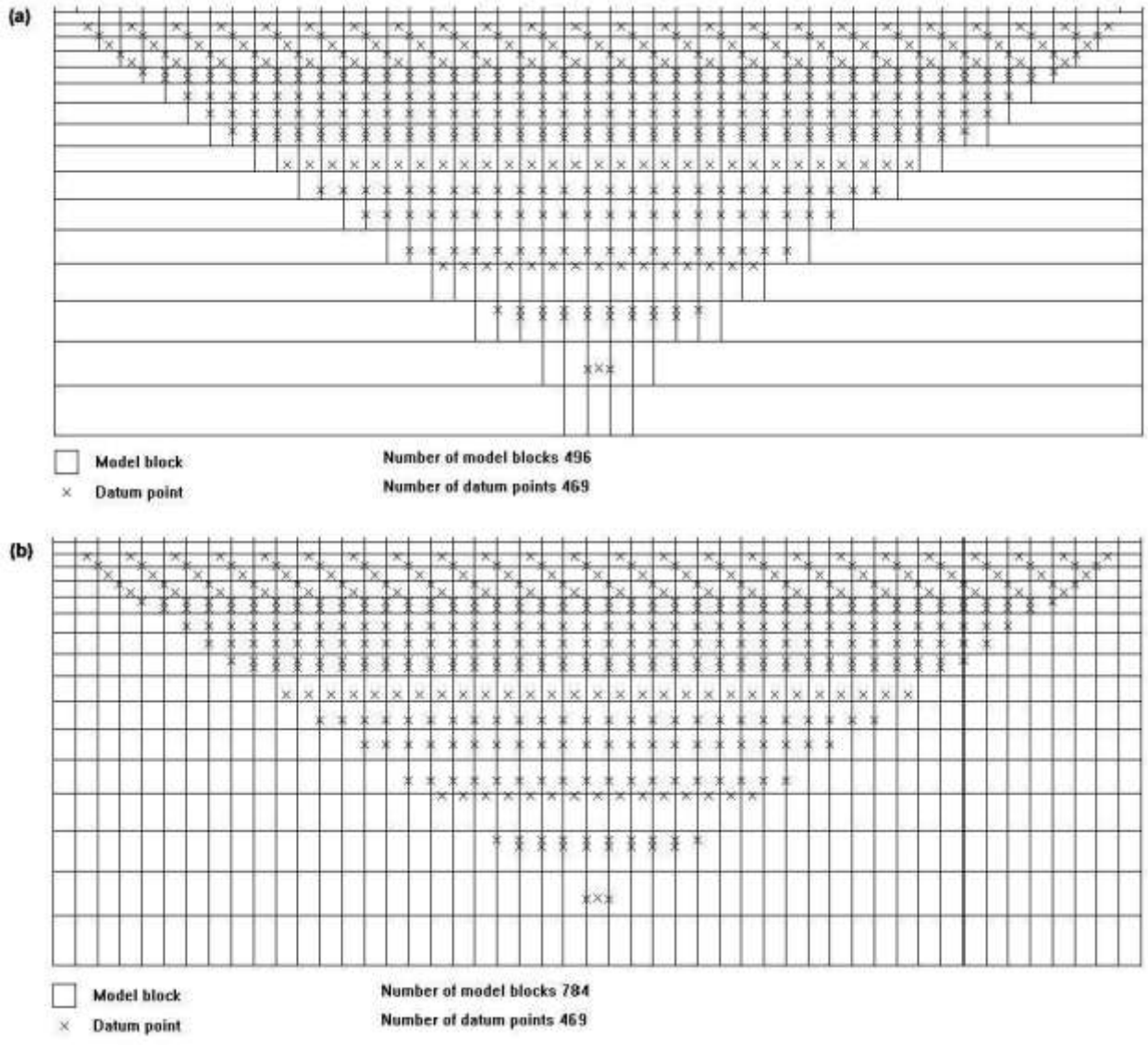

Figure 3.5: (a), (b) are two possible arrangements of the blocks used in a 2-D model together with the datum points in the pseudosection (Edwards, 1977).

The program calculates the apparent resistivity values by the finite-difference method and compares these to the measured data by iteration to reduce the difference between them. During iteration, the modeled resistivity values will be adjusted until the calculated apparent resistivity values of the model agree with the actual measurements. The iteration stops only when the inversion process converges, as measured by the root-mean-squared (RMS) error (i.e., when the RMS error either falls to acceptable limits, usually less than 5% or when the change between RMS errors for consecutive iterations becomes infinitesimally small). However, the model with the lowest possible RMS error can sometimes show a large unrealistic value in the model resistivity values and therefore, might not always be the best model geologically. Hence, the most prudent approach is to choose the model at the iteration when RMS error does not change significantly, between the 3rd and 5th iterations. A model was accepted at the iteration beyond which the RMS error does not change significantly (usually between the 8th and 10th iteration). The final output displayed after the inversion was the measured and calculated apparent resistivity pseudo-sections and the inverse model showing true depth and true formation resistivity.

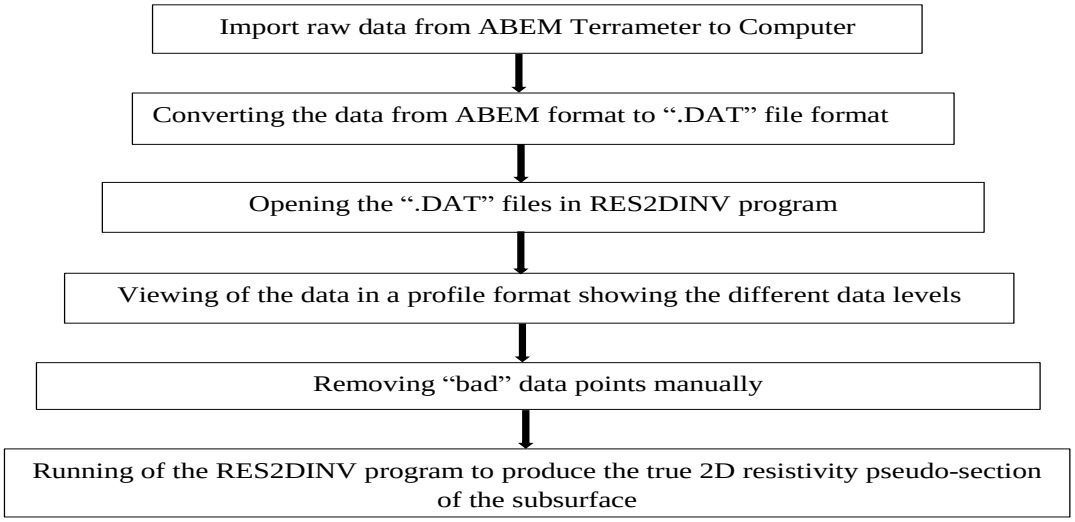

Figure 3.6: 2D Imaging data processing flow chart.

CHAPTER FOUR

RESULTS AND DISCUSSION

4.1 Results and Geological Interpretation

Interpretation of resistivity data consists of two steps: a physical interpretation of the measured apparent resistivity data, resulting in a physical model, and a geological interpretation of the resulting physical parameters based on geological controls (Loke, 2000). The true resistivity structure has been interpreted using automatic 2D smoothness constrained least-squares inversion. A useful amount of information can be extracted from a pseudo section by careful inspection of the contour pattern and apparent resistivity values, particularly if some geological control is available. Contours tend to follow horizontal or gently sloping boundaries between strata of different resistivities, though steep contacts are much smoother. Steep boundaries can be identified using some of the gradient measurements provided they show a strong resistivity contrast. Contour peaks and troughs are correctly positioned relative to the subsurface features giving rise to them, and some estimate of depths at which boundaries occur may be made. If there are marked departures from "two-dimensionality," then the contour pattern may be affected by resistivity contrasts close to, but outside the plane of the section.

Generally, even if the acquisition of a data set is straightforward due to the improvements in resistivity data acquisition systems, data interpretation involves many factors which may be difficult when some parameters in the inversion procedure are neglected. Such parameters include the stability, robustness, and uniqueness of the inversion algorithm (Cardarelli & Fischanger, 2006).

4.2 Correlation of 2D Tomography with Lithological Borehole Data

Boreholes are a necessary and reliable source of primary data through data acquisition methods can be more expensive. The electrical resistivity imaging interpretations provide secondary information and the data acquisition method is less expansive. To better constrain the geophysical interpretation in the characterization of coal seam with the underlying geology, previous geological information obtained from the study area (see Table 4.1) and the preliminary investigations carried out in the study area were used to qualitatively and quantitatively interpret the 2D geoelectrical survey data acquired for the various profiles. Stratigraphic column of Area A represents exposed lithological units at nearby mining site where profile 1 and 2 were taken. While, stratigraphic column of Area B represents exposed lithological units merged with inferred lithological units of Area A for the barren area where profile 3 to 9 were taken (see figure 4.1).

Table 4.1: Lithological units of Odagbo Coal seam adapted from (Umeji, 2005).

Lithology	Thickness (m)	Depth (m)
Lateritic overburden	4	4
Weathered interlamination of silt and shale, flaser and lenticular-bedded	10	14
Parallel-laminated silty-shale, (heterolithic) containing three depositional units with erosional bases	2.2	16.2
Non-laminated, carbonaceous black shale. Base, erosional with rip-up clasts	0.5	16.7
Wavy-laminated, lenticular-bedded silty-shale (heterolithic) sharp base	1.2	17.9
Lignitic coal	2.2	20.1

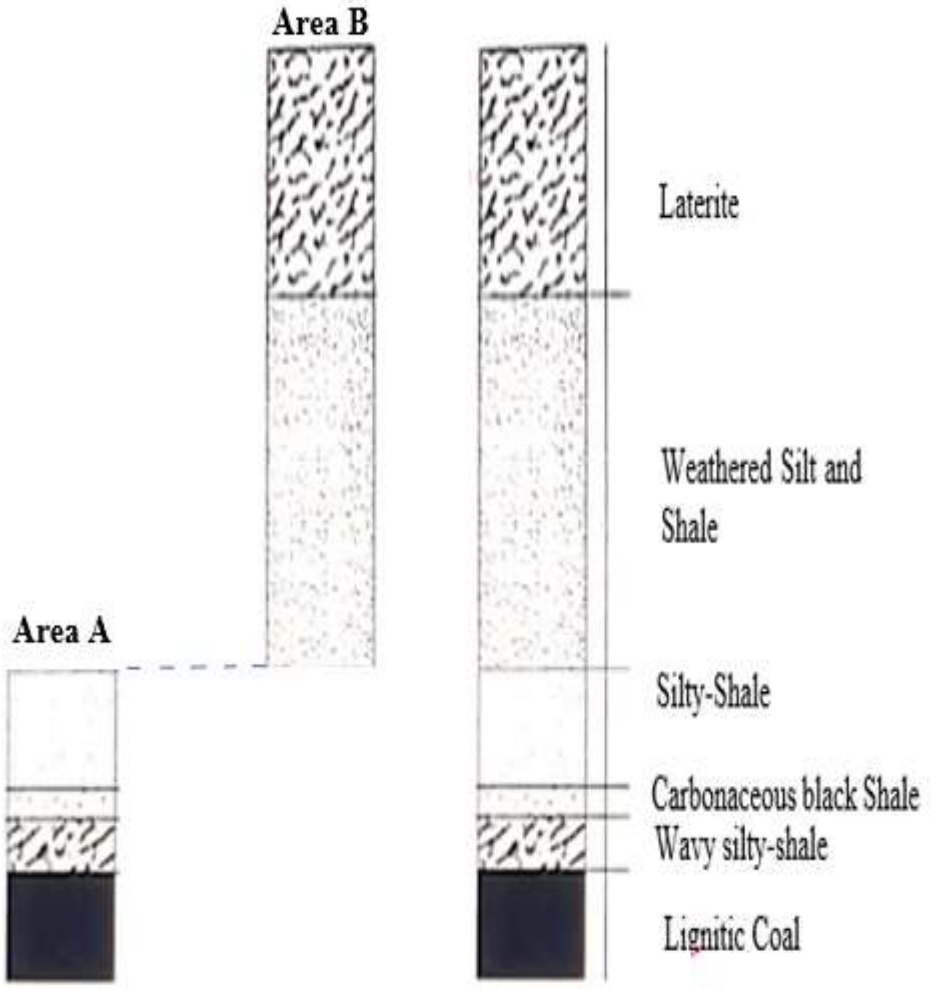

Figure 4.1: Stratigraphic column of Odagbo Coal seam.

4.3 Result of Processed Field Data

4.3.1 Profile 1

Figure 4.2 shows the inversion result of profile 1. The maximum depth of the electrode's penetration is 28.7 m. The resistivity model reveals a layer with resistivity values ranging from 363 Ωm to 3923 Ωm with a depth of about 6 m from surface. This layer is composed of silty-shale, shale and carbonaceous black shale. Underlying the overburden is a moderately high resistive layer from a depth of about 6 m to 20 m with resistivity value varying from about 3 Ωm to 363 Ωm which spreads along the entire profile. Coal seam was interceptedat a lateral distance of 90 m, 105 m from a varying depth of 6 m to 20 m with resistivity value varying from 49 Ωm to 195 Ωm. Also, a small section of low resistivity values ranging from about 3 Ωm to 26 Ωm is indicative of wet clay. Below this layer is the fresh bedrock with high resistivity values ranging from 363 Ωm to 3923 Ωm which is likely composed of carbonaceous black shale to silty-shale.

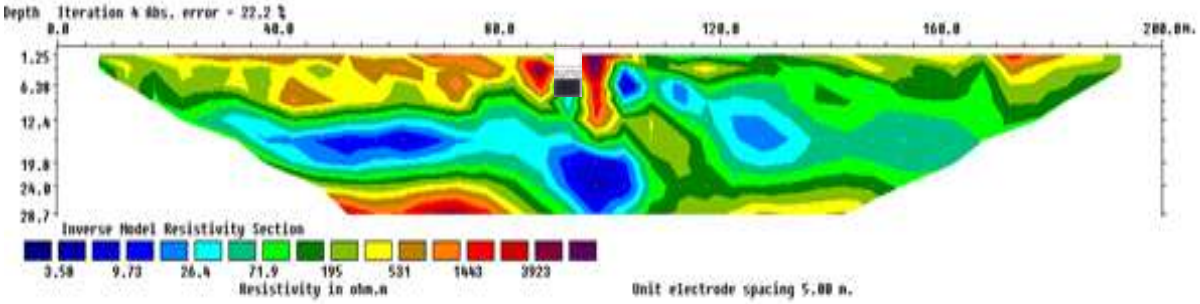

Figure 4.2: Inverse resistivity model of profile 1.

4.3.2 Profile 2

Figure 4.3 shows the inversion result of profile 2. The maximum depth of the electrodes penetration is approximately 29 m. The resistivity model reveals a layer with resistivity values ranging from about 252 Ωm to 2648 Ωm for a depth of about 6 mwhich is likely composed of silty-shale, shale and carbonaceous black shale. Along a lateral distance of 160 m to 180 m is a small section of high resistivity varying from 403 Ωm to 2648 Ωm which indicates sandstone intrusion into the subsurface. Underlying the overburdenfrom a depth of about 6 m to 25 m between the lateral distance of 50 m to 90 m and 110 m to 130 m along the profile is a low resistive section with resistivity values ranging from about 12 Ωm to 115 Ωm. This low resistive section might be water infiltration from acid mine drainage. Probable coal seam occurs within resistivity values varying from about 84 Ωm to 184 Ωm from a depth of about 6 m to 25 m which is masked with the infiltrated water. Below this layer is the fresh bedrock with high resistivity layers of resistivity values ranging from 252 Ωm to 2648 Ωm and is likely composed of carbonaceous back shale to silty-shale.

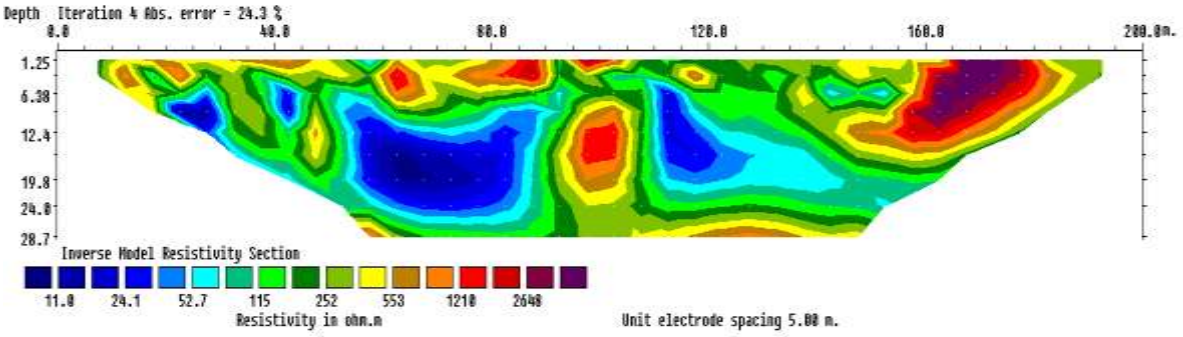

Figure 4.3: Inverse resistivity model of profile 2.

4.3.3 Profile 3

Figure 4.4 shows the inversion result of profile 3. The maximum depth of the electrode's penetration is 28.7 m. The resistivity model shows high resistivity values ranging from about 921 Ωm to 4018 Ωm which constitute the top soil and composed of lateriteand sandy clay to a depth of about 6 m from surface. Underlying this layer is a moderately high resistive layer from a depth of about 6 m to 28.7 m with resistivity values varying from about 129 Ωm to 1585 Ωm. This layer is likely composed of silt, silty-shale, shale and carbonaceous black shale. There is also an occurrence of sections of high and low resistivity values ranging from 563 Ωm to 1585 Ωm and 129 Ωm to 563 Ωm, respectively. The high-resistive sections are likely sandstones, while the low-resistive sections are likely shales hosting the probable coal seam. Coal seam occurs within this layer with resistivity values ranging from about 454 Ωm to 563 Ωm.

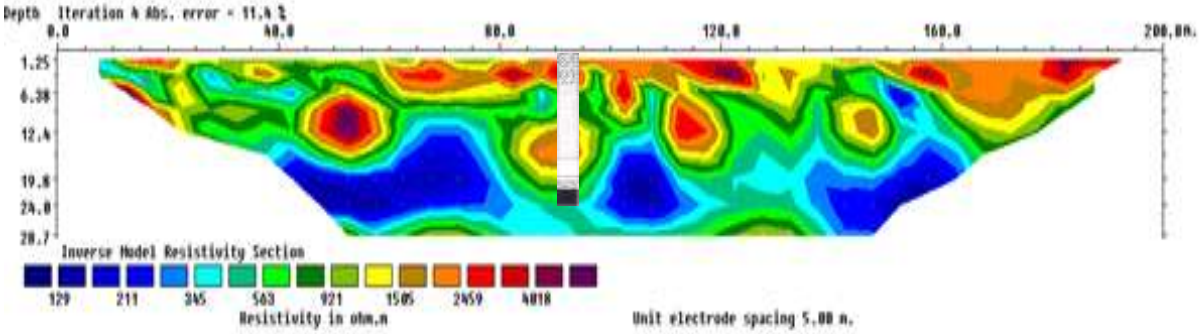

Figure 4.4: Inverse resistivity model of profile 3.

4.3.4 Profile 4

Figure 4.5 shows the inversion result of profile 4. The maximum depth of the electrodes penetration is 28.7 m. The resistivity model shows high resistivity values ranging from about 546 Ωm to 20715 Ωm to a depth of about 6 m from surface. This layer is composed of lateritic clayey sand. Underlying this layer is a moderately high resistive layer from a depth of about 6 m to 28.7 m with resistivity values varying from about14 Ωm to 6164 Ωm. This layer is likely composed of silt, silty-shale, shale and carbonaceous black shale. There is also an occurrence of a section of low resistivity values ranging from 14 Ωm to 546 Ωm. The low resistive-section is probably clay saturated with waterand probable coal seam with resistivity values ranging from about 354 Ωm to 546 Ωm at shallow depth.

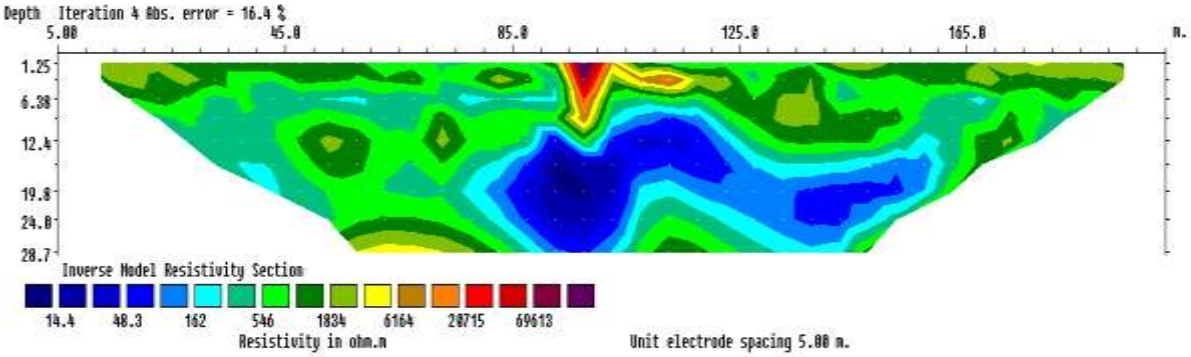

Figure 4.5: Inverse resistivity model of profile 4.

4.3.5 Profile 5

Figure 4.6 shows the inversion result of profile 5. The maximum depth of the electrodes penetration is 28.7 m. The resistivity model shows the top soil with high resistivity values ranging from about 546 Ωm to 50316 Ωm to a depth of about 9 m from surface. This layer is likely composed of lateritic clayey sand. Underlying this layer is a layer with resistivity values varying from about6 Ωm to 3883 Ωm from a depth of about 9 m to 28.7 m. This layer is likely composed of silt, silty-shale, shale and carbonaceous black shale. There is also an occurrence of section of low resistivity values ranging from 6 Ωm to 300 Ωm within this layer. The low-resistive section is probablysandy clay saturated with water and probable coal seam with resistivity values ranging from about 192Ωm to 300 Ωmmay occur at a shallow depth.

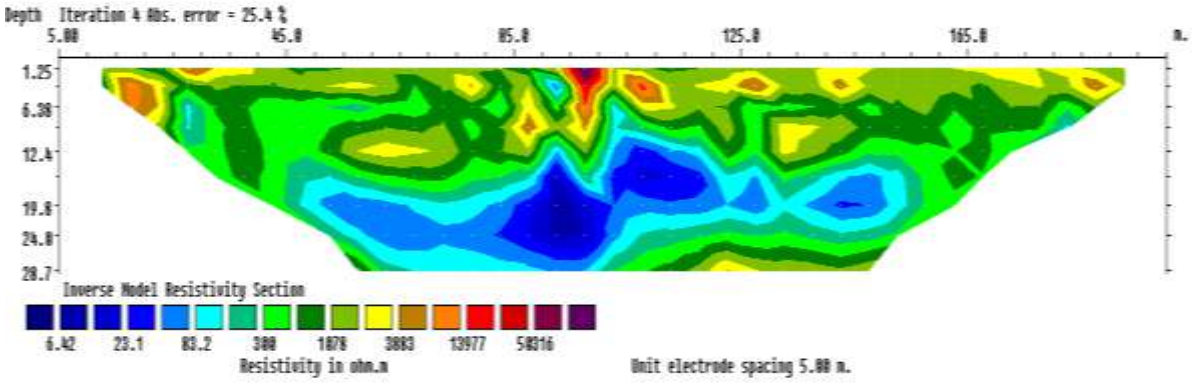

Figure 4.6: Inverse resistivity model of profile 5.

4.3.6 Profile 6

Figure 4.7 shows the inversion result of profile 6. The maximum depth of the electrodes penetration is 28.7 m. The resistivity model shows the top soil with high resistivity values ranging from about 681Ωm to 15770 Ωm to a depth of about 9 m from surface. This layer is likely composed of lateritic clayey sand which intrudes the subsurface at lateral distance of 25 m to 35 m and 170 m to 175 m. Underlying this layer is a layer with resistivity values varying from about1 Ωm to 681 Ωm from a depth of about 9 m to 28.7 m. This layer is likely composed of silt, silty-shale, shale and carbonaceous black shale. There is an occurrence of section of low resistivity values ranging from greater than 1 Ωm to 142 Ωm within this layer. The low-resistive section is probablysandy clay saturated with water and probable coal seam with resistivity values ranging from about 84Ωm to 412 Ωmmay occur at a shallow depth. Also, below this layer at a lateral distance of 85 m and depth between 19.8 m to 28.7 m is high resistivity layer with resistivity values ranging from about 681Ωm to 15770 Ωmwhich may compose of carbonaceous sandstone.

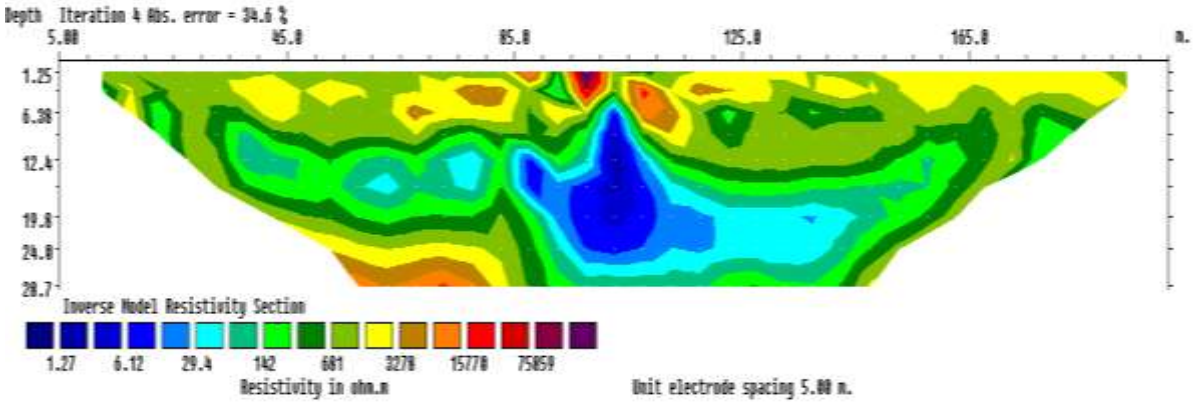

Figure 4.7: Inverse resistivity model of profile 6.

4.3.7 Profile 7

Figure 4.8 shows the inversion result of profile 7. The maximum depth of the electrodes penetration is 28.7 m. The resistivity model shows the top soil with high resistivity values greater than 741Ωm to a depth of about 12 m from surface. This layer is likely composed of intercalation of sand and lateritic clay which also intrudes the subsurface at lateral distance of 30 m to 35 m and 160 m to 175 m. Underlying this layer is a layer with resistivity values varying from about0 Ωm to 741 Ωm from a depth of about 12 m to 28.7 m. This layer is likely composed of silt, silty-shale, shale and carbonaceous black shale. There is an occurrence of section of low resistivity values ranging from greater than 0 Ωm to 49 Ωm within this layer. The low-resistive section is probablysandy clay saturated with water and probable coal seam with resistivity values ranging from about 49Ωm to 245 Ωmmay occurat a shallow depth. Also, below this layer at a depth between 19.8 m to 28.7 m is high resistivity layer with resistivity values ranging from about 741Ωm to 6238 Ωmwhich may compose of carbonaceous sandstone.

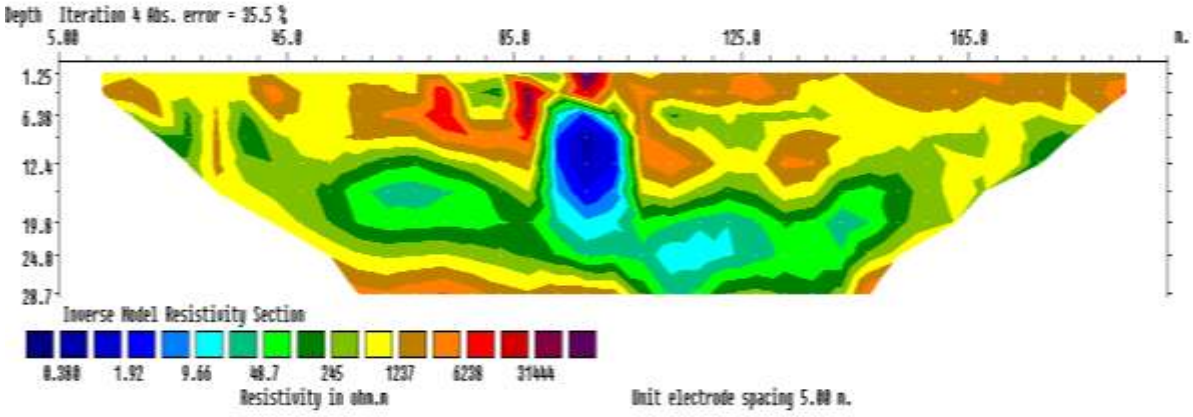

Figure 4.8: Inverse resistivity model of profile 7.

4.3.8 Profile 8

Figure 4.9 shows the inversion result of profile 8. The maximum depth of the electrodes penetration is 28.7 m. The resistivity model shows the top soil with high resistivity values greater than 1624Ωm to a depth of about 9 m from surface. This layer is likely composed of lateritic clayey sand. Underlying this layer is a layer with resistivity values varying from about0 Ωm to 1624 Ωm from a depth of about 9 m to 25 m which is likely composed of silty-shale, shale and carbonaceous black shale. This layer is likely composed of silt, silty-shale, shale and carbonaceous black shale. There is an occurrence of section of low resistivity values ranging from 0 Ωm to 112 Ωm within this layer. The low-resistive section is probablywet sandy clay. Probable coal seam with resistivity values ranging from about 112Ωm to 549 Ωmmay occur at a shallow depth. Also, below this layer at a depth between 24.8 m to 28.7 m is high resistivity layer with resistivity values greater than 1624 Ωmwhich may compose of carbonaceous sandstone.

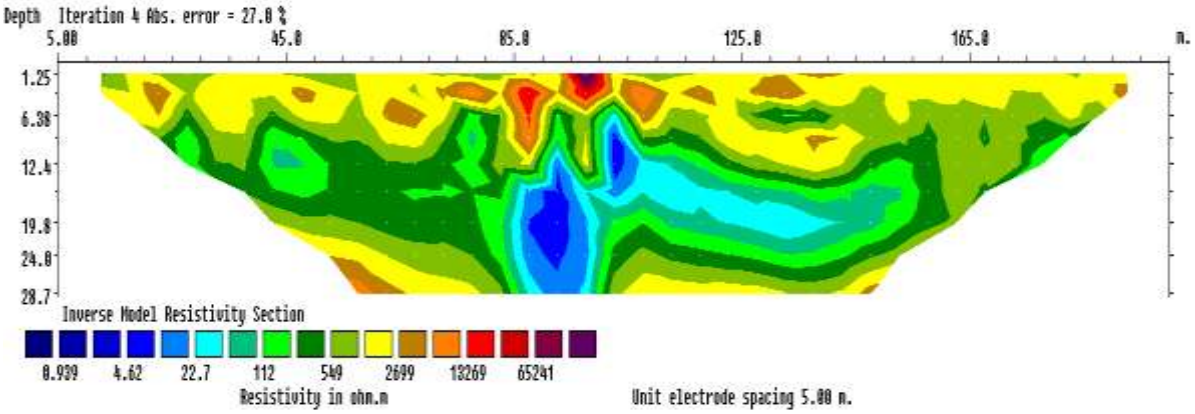

Figure 4.9: Inverse resistivity model of profile 8.

4.3.9 Profile 9

Figure 4.10 shows the inversion result of profile 9. The maximum depth of the electrodes penetration is 28.7 m. The resistivity model shows the top soil with high resistivity values greater than 2244Ωm to a depth of about 9 m from surface. This layer is likely composed of lateritic clayey sand. Underlying this layer is a layer with resistivity values varying from about0 Ωm to 2244 Ωm from a depth of about 9 m to 25 m which is likely composed of silty-shale, shale and carbonaceous black shale. There is an occurrence of section of low resistivity values ranging from 0 Ωm to 119 Ωm within this layer. The low-resistive section is probablywet sandy clay. Probable coal seam with resistivity values ranging from about 123 Ωm to 525 Ωm may occur at a shallow depth. Also, below this layer at a depth between 24.8 m to 28.7 m is high resistivity layer with resistivity values greater than 1620Ωm which may compose of carbonaceous sandstone.

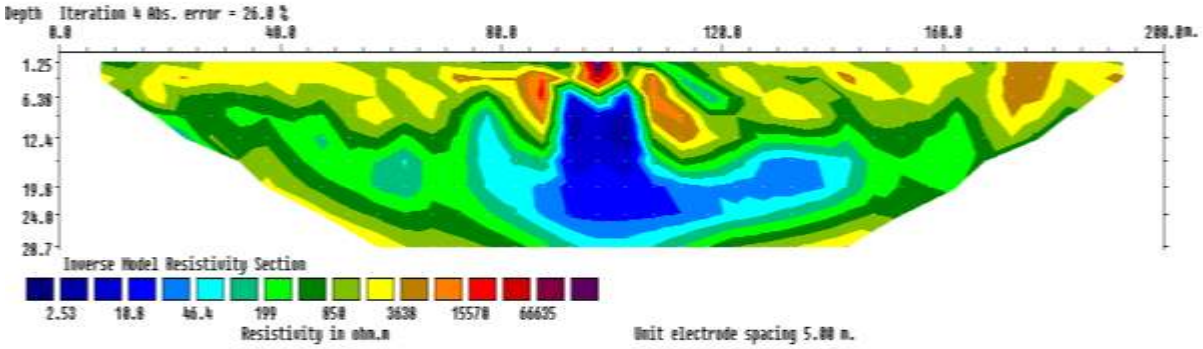

Figure 4.10: Inverse resistivity model of profile 9.

The 2D electrical resistivity slices were collated into a single 3D data set, so as to present a 3D tomography of the study area. The collated data from RES2DINV software were then processed into 3D pseudo-sections using the RES3DINV software. This collated data contained a 41x6 grid electrode with 233 electrode points. The inversion of this data set was carried out on a corei7 microcomputer and it took some minutes for the program to converge to a satisfactory model. The inversion process converged after seven (7) iteration and the inversion model consisted of 1782 blocks. The 3D pseudo-sections are presented as shown in figure 4.11.

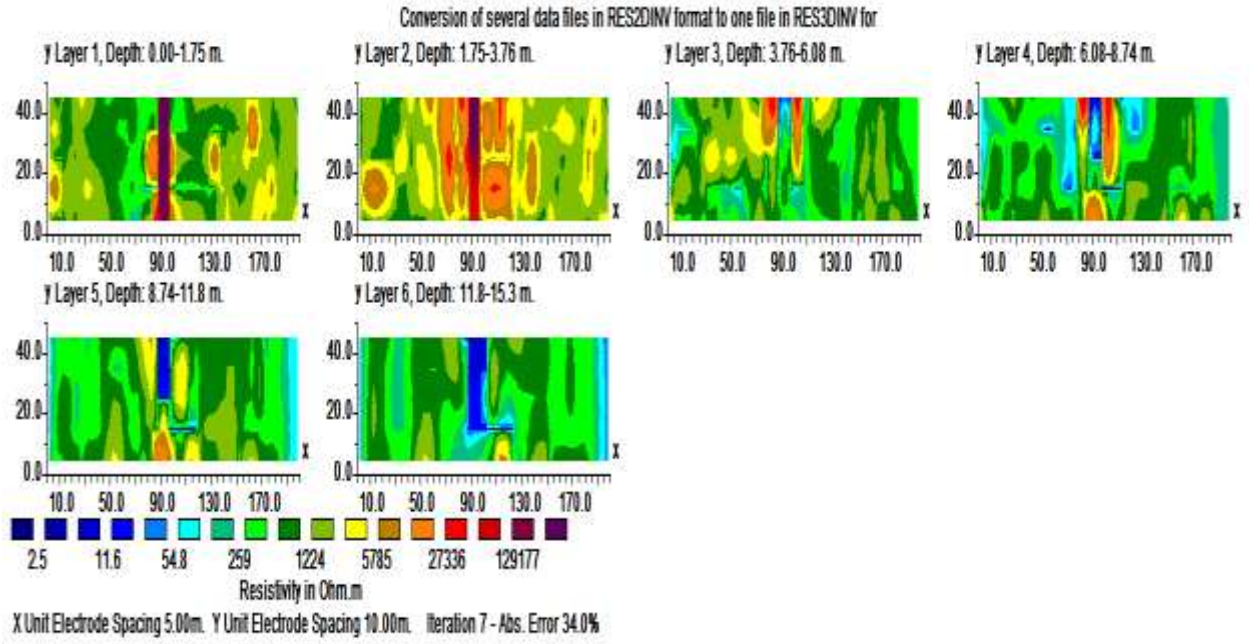

Figure 4.11: 3D pseudo-sections horizontal slice of Study Area.

The horizontal slice contained a total number of six (6) layers with amaximum depth of 15 m.

4.4 Correlation of Profiles for the Detection of Continuity of the Subsurface Structures

The resistivity model of each profile taken was aligned as in the map illustrating the profiles layout with the aim of ascertaining the continuity of subsurface structures and by inference, detect the trend of coal deposit.

Coal occurs in strata,applying Steno's Principle of lateral continuity which states that "Material forming any stratum were continuous over the surface of the earth unless some other solid bodies stood in the way (Stovall, 1955)."Where the lateral continuity of the strata is missing, erosion or faulting can be inferred. This principle has application to the correlation of strata.The resistivity models of merged profiles are given in Figure 4.12-13 below.

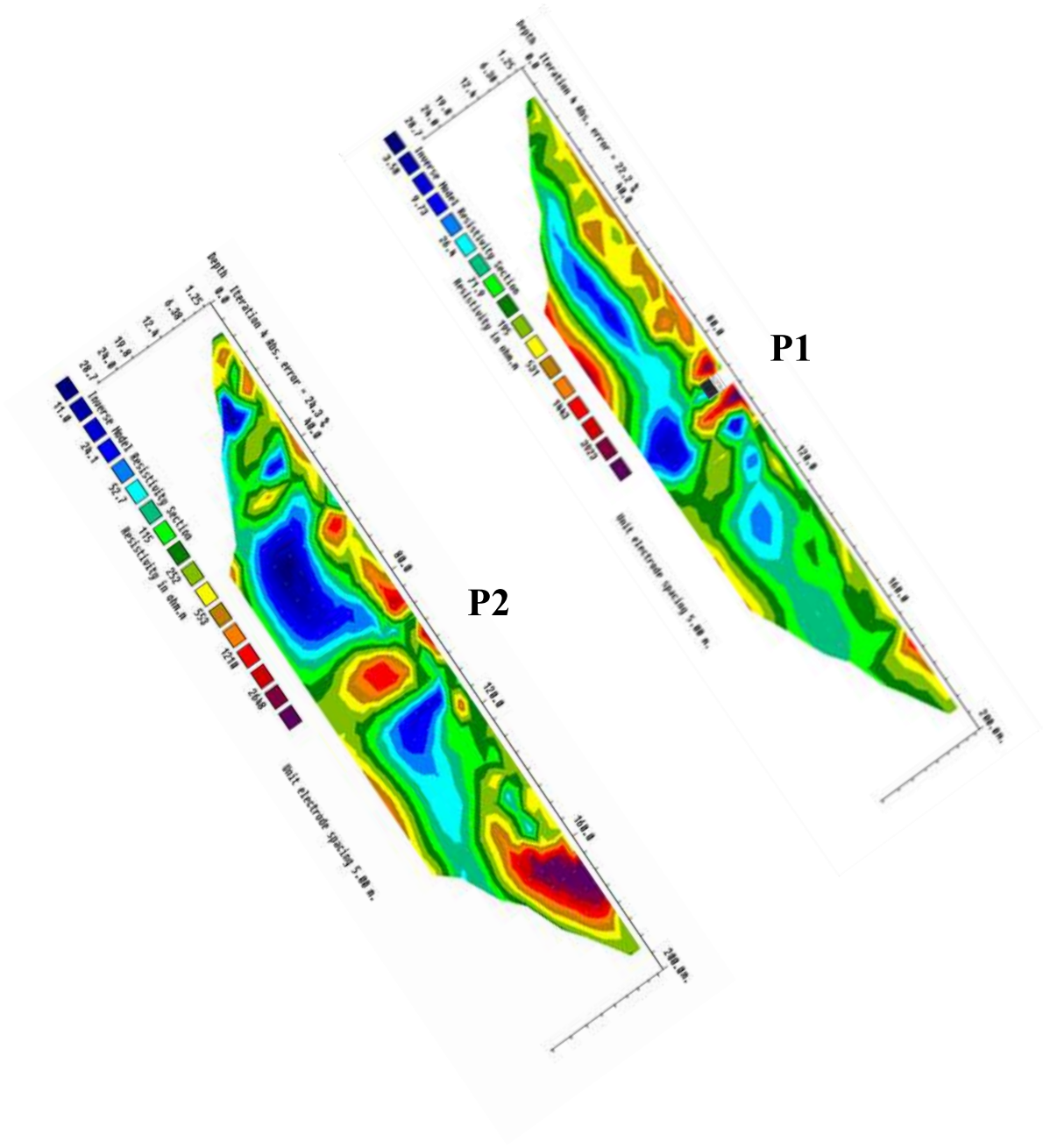

Figure 4.12: 2D Resistivity inversions of two profiles in NW – SE direction merged together, located near open pit mine site.

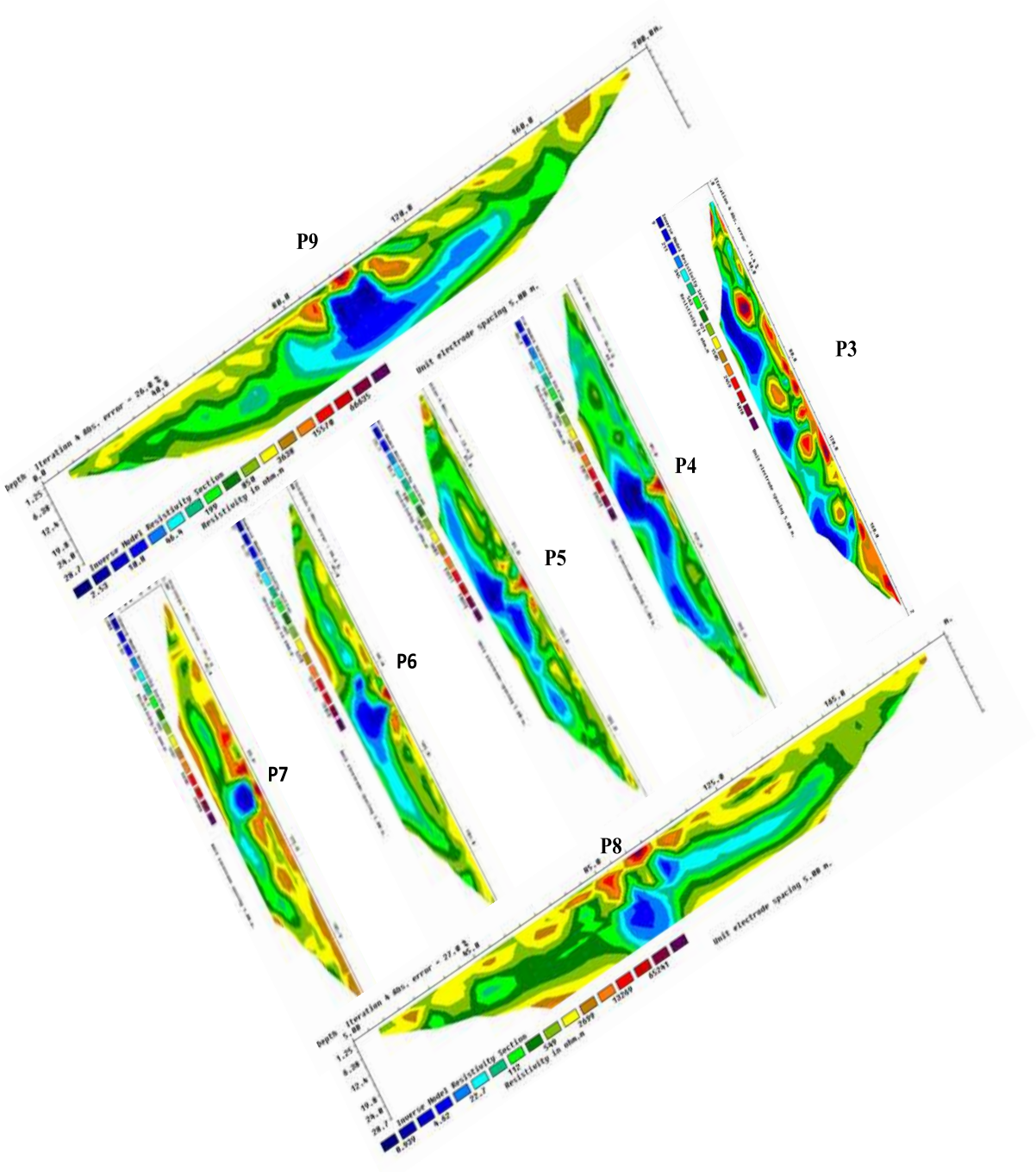

Figure 4.13: 2D Resistivity inversions of five profiles in NW – SE direction merged with two profiles in E – W direction, located in an unexcavated land.

4.5 Discussion

According to Umeji (2005), the regional geology of Odagho is underlain by two major formations, the Manu formation and the Ajali formation. The Manu formation is the coal-

bearing formation. Both the lithological units observed fromthe study area, and the response of coal seams on account of contrast in their electrical properties to the surrounding medium was used as a guide to characterizing coal seams in the study area. This investigation revealed a minimum of three geo-electric sections and from all profiles, distinct layers were observed that varied in both depth and resistivity values.

To be able to determine the strike direction of the coal seam, profiles 1 and 2 were taken at an open coal mine. This also helped to determine the resistivity range and bearing layer of the coal seam. The direction of the mine tunnel can be seen from profiles 1 and 2, and the coal-bearing layer lies within that depth (6 - 25 m) with a resistivity range of 49 Ωm to 200 Ωm. The low resistivity values could be attributed to tunnels being infilled with water. These two profiles were used as a control to correlate with the other profiles taken at the barren sites.

Profiles 3-9 were taken at a barren area in which the artisan miners intend to further investigate coal. It can be observed from each profile, the continuation of the tunnel which was observed in both profiles 1 and 2. This continuation can be attributed to the fact that over time, erosion may have played an effect and lead to the expansion of the tunnel. As a result of this, it is inferred that the coal seam could most probably be at the tunnel direction, which is approximately at a depth of 12 – 25 m. This also correlates with the observed log and also the resistivity range of coal (67- 549 Ωm). The coal seam strike direction was observed to be in the NE-SW direction. Profiles laid parallel to each other were merged to observe the continuity of geologic materials and invariably obtain the strike direction of coal occurrence in the study area. Profiles 1, 2,3, 4, 5, 6, and 7, laid in the NW - SE direction, were aligned alongside Profiles 8 and 9, laid in the E - W direction.

Generally, the result of the 2D resistivity inversion of field dataset resolved relatively similar structures in the range of investigation depth within the survey area characterized by trends of “high resistivity-low resistivity-high resistivity.” The top layer consists of earth materials with high resistivity values greater than 700 Ωm. This layer probably consists of lateritic to sandy clay. It has a thickness of about 6 m. Below the topsoil is the second layer with moderate resistivity values lower than 2200 Ωm except for profiles 1 and 2 with resistivity values between 70 Ωm to 400 Ωm. This layer may consist of highly weathered rocks with shales and coal seams. The 3D map further showed and justified the 2D results. It was seen that the coal bearing layer is at a depth of 6 - 13 m with resistivity values in the range of 10 - 300 Ωm. This relatively low resistivity value can be attributed to the coal bearing layer containing water.

CHAPTER FIVE

CONCLUSION AND RECOMMENDATION

5.1 Conclusion

Thus, the research on electrical resistivity imaging at an old coal mine working in Odagbo village, Kogi, Nigeria, have obtained the following results:

1. Geoelectrical sections representing subsurface earth materials closely related with resistivity values ranging from 0 Ωm to 75859 Ωm from the surface to a depth of 28.7 m. Three distinctive layers namely; the overburden layer with resistivity above 700 Ωm and composed of sandy-lateritic sediments reaching 6m from surface, the weathered layer with resistivity below 2200 Ωm and composed of Shales to Carbonaceous Shales from the depth range of 6 – 25 m, and the fresh bedrock with resistivity above 700 Ωm from the depth of about 25 m.

2. The Coal bearing layer is within the weathered layer of the bedrock. The weathered layer composed of Shales which is the host bedrock for the Coal seam. Coal seam resistivity values within the study area were estimated to be ranging from about 67 - 549 Ωm.

3. Areas with very low resistivity values were suggested to be the depth to Coal seam and coal mine voids filled with water for depth between 12-25 m and trending North-East direction of the study area.

5.2 Recommendations

The ERI method denotes a suitable geophysical tool for subsurface investigation before the mining process. However, it is recommended that further investigation using the seismic reflection tomography method should be conducted to complement and ascertain results obtained using resistivity method.

REFERENCES

Abbass, A., & Mallam, Abu (2013). Investigating the structures within the Lower Benue and Upper Anambra basins, Nigeria, using first Vertical Derivative, Analytical Signal and (CET) centre for exploration targeting plug-in, *2*(5), 104–112.https://doi.org/10.11648/j.earth.20130205.11

ABEM, Instrument AB., (2010). *Terrameter SAS1000/4000 LUND Imaging System Instruction Manual.* Sunbyberg, Sweden: ABEM.

Adeleye D.R. (1989). The Geology of the Mid-Niger Basin. In: Kogbe CA (ed) Geology of Nigeria, 2nd edn. Elizabethan Publishing Co., Lagos, pp. 283–287.

Adetona, A. A., & Abu, M. (2013). Investigating the structures within the lower Benue and upper Anambra Basins, Nigeria, using first vertical derivative, analytical signal and (CET) Center for exploration targeting plug-in. *Earth Sci, 2*(5), 104-112.

Adigun, O. D., & Kayode, S. (2019). Environmental assessment of surface water/coal deposit interaction from trace minerals in Okaba coal field, Okaba North Central Nigeria. *FUOYE Journal of Engineering and Technology, 4*(2).

Agagu, O. K., & Adighije, C. I. (1983). Tectonic and sedimentation framework of the lower Benue Trough, southeastern Nigeria. *Journal of African Earth Sciences, 1*(3-4), 267-274.

Agagu, O., & Ekweozor, C. (1982). Source rock characteristics of Senonian shales in the Anambra Syncline, Southern Nigeria. *Journal of Mining and Geology*, *19*(2), 51-61.

Agagu, O.K., Fayose, E. A. & Petters, S. W. (1985). "Stratigraphy and sedimentation in the Senonian Anambra Basin of Eastern Nigeria", *Journal of Mining and Geology*, 22: 25–36.

Aizebeokhai, A. P. (2010). 2D and 3D geoelectrical resistivity imaging: Theory and field design. *Scientific Research and Essays, 5*(23), 3592-3605.

Aizebeokhai, A. P., & Oyeyemi, K. D. (2014). The use of the multiple-gradient array for geoelectrical resistivity and induced polarization imaging. *Journal of Applied Geophysics*, *111*, 364-376.

Aja A. & Emeribe, A. (2000). Policy and Contending Issues in Nigerian National Development Strategy, Enugu.

Akande, S. O., Hoffknecht, A., & Erdtmann, B. D. (1992). Rank and petrographic composition of selected Upper Cretaceous and Tertiary coals of southern Nigeria. *International Journal of Coal Geology*, *20*(3-4), 209-224.

Akande, S. O., Ogunmoyero, I. B., Petersen, H. I., & Nytoft, H. P. (2007). Source rock evaluation of coals from the Lower Maastrichtian Mamu Formation, SE Nigeria. *Journal of Petroleum Geology, 30*(4), 303-324.

Akande, S., & Mocke, A. (1993). Tectonic and sedimentation framework of the lower Benue Trough, southeastern Nigeria. *Journal of African Earth Sciences, 17*(4), 445-456.

Akujor, C. E., Ogungbenro, O. A., Mejeha, I., Nwofor, O., & Alozie, G. A. (2011). The state of energy supply in nigeria: Need for more efficient utilization of fuelwood resources. *Advances in Science and Technology, 5*(1S).

Ameh, E. (2013). Multivariate statistical analyses and enrichment of heavy metal contamination of soil around Okaba coal mine. *American Eurasian Journal of Agronomy, 6*, 9-18.

Anderson, N. L., Croxton, N., Hoover, R., & Sirles, P. (2008). Geophysical methods commonly employed for geotechnical site characterization. *Transportation Research Circular*(E-C130).

Anyanwu, N., & Arua, I. (1990). Ichnofossils from the Imo Formation and their paleoenvironmental significance. *Journal of Mining and Geology, 26*(1), 1-4.

Arjwech, R., & Everett, M. E. (2015). Application of 2D electrical resistivity tomography to engineering projects: Three case studies. *Songklanakarin Journal of Science & Technology, 37*(6), 675 – 681.

Arjwech, R., Everett, M., Briaud, J. L., Hurlebaus, S., Medina, C. Z., Tucker, S., & Yousefpour, N. (2013). Electrical resistivity imaging of unknown bridge foundations. *Near Surface Geophysics, 11*(6), 591-598.

Auken, E., Pellerin, L., Christensen, N. B., & Sorensen, K. (2006). A survey of current trends in near-surface electrical and electromagnetic methods. *Geophysics, 71*(5), G249-G260.

Aweto, E., & Adaikpoh, K. (2014). Observations from square array resistivity response over Ezimo Coal Field, southeastern Nigeria. *Research Journal of Environmental and Earth Sciences, 6*(2), 90-95.

Bankole, S., Dublin-Green, C., Opatola, A., Olaniran, M., & Akintola, A. (2016). Petrographic and optical cathodoluminescence study of detrital quartz: Provenance indicator for the sediments of the campanian Lokoja-Basange formation, Anambra Basin, Nigeria. *Ife Journal of Science, 18*(4), 861-870.

Batayneh, A. T. (2006). Resistivity Tomography as an aid to planning gas pipeline construction, Risha area, North-Eeast Jordan. *Near Surface Geophysics, 4*(5), 313-319.

Benkhelil, J. (1987). Cretaceous deformation, magmatism, and metamorphism in the Lower Benue Trough, Nigeria. *Geological Journal, 22*(S2), 467-493.

Benkhelil, J. (1989). The origin and evolution of the Cretaceous Benue Trough (Nigeria). *Journal of African Earth Sciences (and the Middle East), 8*(2-4), 251-282.

Beresnev, I. A., Hruby, C. E., & Davis, C. A. (2002). The use of multi-electrode resistivity imaging in gravel prospecting. *Journal of Applied Geophysics, 49*(4), 245-254.

Birol, F. (2008). World energy outlook. *Paris: International Energy Agency, 23*(4), 329.

Board. (2009). *Clean coal technologies: Accelerating commercial and policy drivers for deployment.* OECD/IEA.

Board. (2012). The Global Value of Coal. *IEA (Paris, 2012).*

Borishade, A. B., Hanan, A. H. M. A., Kehinde, L. O., Oluwole, A. F., & Oshin, O. (1985). Elemental composition of Nigerian coals. *Energy, 10*(1), 35-39.

Brown, C. E. (2012). *World energy resources: international geohydroscience and energy research institute.* Springer Science & Business Media.

Burke, K. C., Dessauvagie, T. F. J., & Whiteman, A. J. (1972). Geological history of the Benue valley and adjacent areas. *African geology, 1*(8), 7-2.

C.I.A.B., Coal Industry Advisory Board (2008). Clean Coal Technologies: Accelerating Commercial and Policy Drivers for Deployment, CIAB, International Energy Agency, Paris.

Cardarelli, E., & Fischanger, F. (2006). 2D data modelling by electrical resistivity tomography for complex subsurface geology. *Geophysical Prospecting, 54*(2), 121-133.

Carter, J. D., Barber, W., Tait, E. A. & Jones, G. P. (1963). The Geology of Parts of Adamawa, Bauchi and Borno Provinces in Northeastern Nigeria. Bulletin Geological Survey Nigeria, 30, 1 – 108.

Çelik, P. A., Aksoy, D. O., Koca, S. H., Koca, H., &Çabuk, A. (2019). The approach of biodesulfurization for clean coal technologies: a review. *International journal of environmental science and technology, 16*(4), 2115-2132.

Chalikakis, K., Plagnes, V., Guerin, R., Valois, R., & Bosch, F. P. (2011). Contribution of geophysical methods to karst-system exploration: an overview. *Hydrogeology Journal, 19*(6), 1169-1180.

Chambers, J., Wilkinson, P., Penn, S., Meldrum, P., Kuras, O., Loke, M., & Gunn, D. (2013). River terrace sand and gravel deposit reserve estimation using three-

dimensional electrical resistivity tomography for bedrock surface detection. *Journal of Applied Geophysics, 93*, 25-32.

Christine, K. (2015). The Nigeria Coal Atlas Heinrich B'll Foundation. *Berlin (Germany), Heinrich B'll Foundation, Nigeria and Friends of the Earth International, London, UK*, 10.

Chukwu, M., Folayan, C. O., Pam, G. Y., & Obada, D. O. (2016). Characterization of some Nigerian coals for power generation. *Journal of Combustion, 2016*. Article ID 9728278, 11 pages http://dx.doi.org/10.1155/2016/9728278

Cofala, J., Borken-Kleefeld, J., Heyes, C., Klimont, Z., Rafaj, P., Sander, R., & Amann, M. (2011). Emissions of Air Pollutants for the World Energy Outlook 2011 Energy Scenarios.

Cozzi, L., & Gould, T. (2015). World Energy Outlook 2015. *International Energy Agency*.

Dahlin, T. (2000). Short note on electrode charge up effects in DC resistivity data acquisition using multi electrode arrays. *Geophysical Prospecting, 48*(1), 181-187.

Dahlin, T. (2001). The development of DC resistivity imaging techniques. *Computers & Geosciences, 27*(9), 1019-1029.

Dahlin, T., & Loke, M. H. (1997). Quasi-3D resistivity imaging-mapping of three dimensional structures using two dimensional DC resistivity techniques. *3rd EEGS Meeting* (pp. cp-95). European Association of Geoscientists & Engineers.

Dahlin, T., & Zhou, B. (2004). A numerical comparison of 2D resistivity imaging with 10 electrode arrays. *Geophysical prospecting, 52*(5), 379-398.

Damasceno, V. M., Fratta, D., & Bosscher, P. J. (2009). Development and validation of a low-cost electrical resistivity tomographer for soil process monitoring. *Canadian Geotechnical Journal, 46*(7), 842-854.

Daniels, F., & Alberty, R. A. (1966). Physical Chemistry.John Wiley and Sons, Inc.

deGroot-Hedlin, C., & Constable, S. C. (1990). Occam's inversion to generate smooth, two-dimensional models from magnetotelluric data. *Geophysics, 55*(12), 1613-1624.

Edwards, G. A. (2019). Coal and climate change. *Wiley Interdisciplinary Reviews: Climate Change, 10*(5), e607.

Edwards, L.S., (1977), A modified pseudosection for resistivity and induced polarization. Geophysics, 42, 1020-1036.

Ehinola, O. A., Oluwajana, O. A., & Adekoya, A. (2012). Geophysical investigation and reserve estimation of a coal seam in Ute area, southwestern Nigeria. *Petroleum & Coal, 54*(3), 252-259.

Essien, A. U., & Igweonu, E. I. (2014). Coal Based Generation: A Solution to Nigeria Electricity Problem. *International Archive of Applied Sciences and Technology*, *5*(1), 74–80.

Ewing, M. A., Crary, A. P. Peoples J. W. & Peoples, J. A. (1936). Prospecting for Anthracite by the Earth Resistivity Method. *Transactions of the American Mining and Metallurgical Engineers,* Coal Division, Vol. 119, pp 43-483.

Famuboni, A. D. (1996). Maximizing Exploration of Nigeria's Coal Reserves. In: Nigerian Coals: A Resource for Energy and Investments, Famuboni, A. D. (Ed.). Raw Materials Research and Development Council (RMRDC), Abuja, Nigeria, pp. 39 – 62.

Fatoye, F. B., & Gideon, Y. B. (2013). Appraisal of the economic geology of Nigerian coal resources. *Journal of Environment and Earth Science, 3*(11), 25-31.

Fatoye, F. B., Omada, J. I. & Olatunji, J. A. (2012). Quality Assessments and Industrial Usages of Cretaceous Okaba Coal, Anambra Basin, Nigeria. *Journal of Mining and Geology*, 48(1), pp. 81 – 87.

Fayose, E. A. & Ola, P. S. (1990). Radiolarian Occurrences in the Ameki type section, eastern Nigeria. *Journal of mining and geology, 26,* 75-80.

Felix, B. F., & Yomi, B. G. (2013). Appraisal of the Economic Geology of Nigerian Coal Resources. Journal of Environment and Earth Science, 3(11), 25-31.

Francis, W. (1961). *Coal: its formation and composition*. E. Arnold.

Gluskoter, H. J. (1975). Mineral matter and trace elements in coal.

Godio, A., & Naldi, M. (2003). Two dimensional electrical imaging for detection of hydrocarbon contaminants. *Near Surface Geophysics, 1*(3), 131-137.

Griffiths, D. H., & King, R. F. (2013). *Applied geophysics for geologists and engineers: the elements of geophysical prospecting.* Elsevier.

Griffiths, D.H. & Barker, R.D., (1993). Two-dimensional resistivity imaging and modeling in areas of complex geology. *Journal of Applied Geophysics*, 29(3-4), 211-226.

Gupta, R. (2007). Advanced coal characterization: A review. *Energy & Fuels, 21*(2), 451-460.

Hartman, H. L., & Mutmansky, J. M. (2002). *Introductory mining engineering*. John Wiley & Sons.

Hatherly, P. (2013). Overview on the application of geophysics in coal mining. *International Journal of Coal Geology, 114*, 74-84. doi: 10.1016/j.coal.2013.02.006

Ibitoye, F. I., & Adenikinju, A. (2007). Future demand for electricity in Nigeria. *Applied Energy, 84*(5), 492-504.

Jerzykiewicz, T., (1990). Coal geology and its application to coal-bed methane reservoirs: lecture notes for short course, Edmonton, August 20-24, 1990. Alberta Research Council.

Johnson, W. J., Appolonia D., & Monroeville, P. A. (2003). Applications of the electrical resistivity method for detection of underground mine workings. *Forum on Geophysical Technologies for Detection of Underground Mine Voids*, Lexington, Kentucky (pp. 28-30).

Jones, G., Sentenac, P., & Zielinski, M. (2014). Desiccation cracking detection using 2-D and 3-D Electrical Resistivity Tomography: Validation on a flood embankment. *Journal of Applied Geophysics, 106*, 196-211.

Kearey, P., Brooks, M., & Hill, I. (2002). *An introduction to geophysical exploration* (Vol. 4). John Wiley & Sons.

Keller, G. V., & Frischknecht, F. C. (1966). Electrical methods in geophysical prospecting. Pergamon Press Inc., Oxford.

Khatib, H. (2012). IEA world energy outlook 2011'A comment. *Energy policy, 48*, 737-743.

Kim, A. G. (1977). *Laboratory studies on spontaneous heating of coal: A summary of information in the literature* (Vol. 8756). Department of the Interior, Bureau of Mines.

Kim, A. G. (1978). *Experimental studies on the origin and accumulation of coalbed gas* (Vol. 8317). Department of the Interior, Bureau of Mines.

Kirchhoff, G. (1857). LIV. On the motion of electricity in wires. *The London, Edinburgh, and Dublin Philosophical Magazine and Journal of Science, 13*(88), 393-412.

Kneisel, C., Emmert, A., & Kostl, J. (2014). Application of 3D electrical resistivity imaging for mapping frozen ground conditions exemplified by three case studies. *Geomorphology, 210*, 71-82. DOI:10.1016/j.geomorph.2013.12.022

Kogbe, C. A. (1976). The Cretaceous and Paleogene sediments of southern Nigeria. *Geology of Nigeria, 1*, 273-82.

Krishnamurthy, N.S., Rao, A.V., Kumar, D., Singh, K.K.K. & Ahmed, S. (2009). Electrical Resistivity Imaging Technique to Delineate Coal Seam Barrier Thickness and Demarcate Water Filled Voids. *Journal of Geological Society of India* 73(5): 639-650.

LaBrecque, D., & Daily, W. (2008). Assessment of measurement errors for galvanic-resistivity electrodes of different composition. *Geophysics, 73*(2), F55-F64.

Langenberg, C.W., Kalkreuth, W., Levine, J.R., Strobl, R., Demchunk, T., Hoffman, G., Jerzykiewicz, T., (1990). Coal geology and its application to coal-bed methane reservoirs: lecture notes for short course, Edmonton, August 20-24, 1990. Alberta Research Council.

Lei, Y. (2015). Application of geophysical technique in the coal mining. *International Journal of Online Engineering* (iJOE), 11 (7), 11-13.

Loke, M. H. (2000). Electrical imaging surveys for environmental and engineering studies; A practical guide to 2-D and 3-D surveys. Electronic version available from http://www.terraplus.com

Loke, M. H. (1999). Electrical imaging surveys for environmental and engineering studies. *A practical guide to, 2*.

Loke, M. H. (2010). RES2DINV ver. 3.59 for Windows XP/Vista/7. Rapid 2-D Resistivity & IP inversion using the least-squares method. *Geoelectrical Imaging 2D & 3D Manual.(Geotomo Software: Penang) Available at: www. geoelectrical. com (verified June 2011).*

Loke, M. H., & Barker, R. D. (1996). Rapid least squares inversion of apparent resistivity pseudosections by a quasi Newton method 1. *Geophysical prospecting, 44*(1), 131-152.

Loke, M. H., Acworth, J. & Dahlin, T. (1999). A comparison of smooth and blocky inversion methods in 2D electrical imaging surveys. *Exploration* Geophysics, 34: 182-187.

Loke, M. H., Chambers, J. E., & Kuras, O. (2011). Instrumentation, electrical resistivity in Solid Earth Geophysics Encyclopedia (2nd Edition), Electrical & Electromagnetic, Gupta, Harsh.

Loke, M. H., Chambers, J. E., Rucker, D. F., Kuras, O., & Wilkinson, P. (2013). Recent developments in the direct-current geoelectrical imaging method. *Journal of Applied Geophysics, 95,* 135-156.

Mallo, S. J. (2012). The Nigerian mining sector: An overview. *Continental Journal of Applied Sciences, 7*(1), 34-45.

Meduni, G., Mondol, D., Ra, E.e, & Nazir, S. (2018). Review of the latest research on coal, environment, and clean technologies. *Rudarsko-geolo'ko-naftni zbornik, 33*(3), 13-21.

Michael, I. O., Oluwakemi, O. A., & Temitope, O. A. (2008). Geoelectric Study of Coal Deposits at Unwana/Afikpo Area of Southeastern Nigeria. *Journal of Applied*

Sciences
Research, 4(11), 1534-1545.

Miller, R. G. (2011). Future oil supply: The changing stance of the International Energy Agency. *Energy Policy*, *39*(3), 1569-1574.

Mills, S. (2014). The energy frontier of combining coal and renewable energy systems. *MITEI.(2016). Commercial EOR projects using anthropogenic carbon dioxide*.

Milsom, J. (2003). *Field geophysics* (Vol. 25). John Wiley and sons.

Mohammed M. A., Adewumi T., Ahmed A. L., & Lawal K. M. (2016). Electrical Resistivity Imaging of a Coal Deposit at Tai Area of Gombe State, North Eastern Nigeria. *Journal of Environment and Earth Science*. ISSN 2225-0948 (Online) Vol.6, No.6, 2016.

Momoh, A., Emmanuel, P. R., Shola, C. O., Mimonitu O., Olusola, J. O., Ayodeji O., (2017). Preliminary Investigation of Trace Elements in Acid Mine Drainage from Odagbo Coal Mine, Northcentral, Nigeria. *Journal of Environment and Earth Science*. ISSN 2225-0948 (Online) Vol.7, No.11, 2017.

Murat, R.C. (1972). "Stratigraphy and Paleogeography of the Cretceous and Lower Tertiary in Southern Nigeria", *In*: Dessauvagie, T.F.J. and Whiteman A.J. (eds.), *African Geology*, 261-269.

Nfor, B. N., Chukwuemeka, L. O., Ogala, J. E., & Olobaniyi, S. B. (2005). An Evaluation of the Artesian System of the Anambra Basin Southeastern Nigeria. *Editorial Advisory Board e*, *15*(2), 140-150.

Nwafor, N. O., Mamah, L. I., Okwara, I. C., Alo, G. A., Okolo, I. T., & Ndulue, I. T. (2017). Geological and Geophysical Investigation of a Late Maastrichtian Coal Seam at Eha-Alumona/Orba Environs, Anambra Basin, Nigeria. *Petroleum & Coal*, *59*(2).

Nwajide, C.S. (1990). Cretaceous Sedimentation and Paleogeography of the Central Benue Though. In: Ofoegbu, C.O; (Ed.), The Benue Tough structure and Evolution International Monograph Series, Braunschweig, pp. 19-38.

Nwaobi, G. C (2012). The Nigerian Coal Corporation: An Evaluation of Production Performance (1960-1987) in Odesola et al., International Journal of Engineering and Applied Sciences Vol. 4 No. 1.

Obaje, N. G. (2009). Geology and Mineral Resources of Nigeria, Lecture Notes in Earth Sciences Springer-Verlag Berlin Heidelberg, pp. 57-68.

Obaje, N. G. & Hamza, H. (2000). Liquid Hydrocarbon Source-rock Potential of Mid-Cretaceous Coals and Coal Measures in the Middle Benue Trough of Nigeria. *International Journal of Earth Sciences: Geologische Rundschau,* 89:130–139.

Obaje, N. G., Funtua, I. I., Ligouis, B., & Abaa, S. I. (1996). Maceral associations, organic maturation and coal-derived hydrocarbon potential in the cretaceous Awgu Formation, Middle Benue Trough, Nigeria. *Journal of African Earth Sciences*, *23*(1), 89-94.

Oberschelp, C., Pfister, S., Raptis, C., & Hellweg, S. (2019). Global emission hotspots of coal power generation. *Nature Sustainability*, *2*(2), 113-121.

Obi, G. C., & Okogbue, C. O. (2004). Sedimentary response to tectonism in theCampanian'Maastrichtian succession, Anambra Basin, southeastern Nigeria. *Journal of African Earth Sciences*, *38*(1), 99-108.

Obi, G. C., Okogbue, C. O. & Nwajide, C. S. (2001). "Evolution of the Enugu Cuesta: A tectonically driven erosional process", *Global journal of Pure and Applied Sciences*, **7:** 321-330.

Obiadi, I. I., Obiadi, C. M., Akudinobi, B. E. B., Maduewesi, U. V., & Ezim, E. O. (2016). Effects of coal mining on the water resources in the communities hosting the Iva Valley and Okpara Coal Mines in Enugu State, Southeast Nigeria. *Sustainable Water Resources Management*, 2(3), 207-216.

Odesola, I. F., Samuel, E., & Olugasa, T. (2013). Coal development in Nigeria: prospects and challenges. *International Journal of Engineering*, *4*(1), 8269.

Ogala, J. E. (2011). Hydrocarbon potential of the Upper Cretaceous coal and shale units in the Anambra Basin, Southeastern Nigeria. *Petroleum and coal*, *53*(1), 35-44.

Ogala, J. E. (2018). Geochemistry of coal and coal bearing strata from the Upper Cretaceous Mamu Formation, Southeastern Nigeria: implications for Paleoredox history. *FUW Trends Sci Technol J*, *3*(2B), 787-796.

Ogala, J. E., Akaegbobi, I. M. & Adaikpoh, E. O. (2005): Sedimentary characteristics of the Maastrichtian fluvial marine sedimentary facies of Anambra Basin. *African Scientist*, Vol. 6, 17-28. (Nigeria; 40%)

Ogala, J., Silvanus, G., & Christanis, K. (2012). Coal petrography, mineralogy and geochemistry of lignite samples from Ogwashi-Asaba Formation, Nigeria. *Journal of African Earth Sciences*, *66-67*(2012), 35-45.

Oguejiofor, G. C. (2010). Using total quality management as a tool for re-engineering coal production in Nigerian Coal Corporation. An Energy Industry case study. Energy Sources, Part B: Economics, Planning, and Policy vol. 5, 2010, pp. 29 – 40.

Ohimain, E. I. (2014). Can Nigeria generate 30% of her electricity from coal. *Int. J. Energy Power Engr*, *3*(1), 28-37.

Ohm, G. S. (1827). *Die galvanische kette: mathematisch.*Berlin: T. H. Riemann.

Oji, J., Idusuyi, N., & Kareem, B. (2012). Coal power utilization as an energy mix option for Nigeria: a review. *American Academic & Scholarly Research Journal, 4*(4), 1.

Oladapo, M. I., Adeoye-Oladapo, O. O., & Alao, T. O. (2008). Geoelectric study of coal deposits at Unwana/Afpiko area of Southeastern Nigeria. *Journal of Applied Sciences Research, 4*(11), 1534-1545.

Olayande J. S., Lamin H. S. & Agba J. O. (2012). Coal deposits in Nigeria: A viable energy option for industrialization. *Energy Commission of Nigeria*.

Omoju, O. E. (2015). Effectiveness of clean coal technologies in global carbon emission mitigation: evidence and summary. *TEMTI Series of Economic Perspectives on Global Sustainability,* 1-13.

Onakoya, A. B., Onakoya, A. O., Jimi-Salami, O. A., & Odedairo, B. O. (2013). Energy consumption and Nigerian economic growth: An empirical analysis. *European scientific journal, 9*(4).

Orajaka, I. P., Onwuemesi, G. E., Egboka, B., & Nwankor, G. I. (1990). Nigerian Coal. *Mining Magazine; (UK)*, pp. 447-448.

Palacky, G. (1988). Resistivity characteristics of geologic targets. *Electromagnetic methods in applied geophysics, 1*, 53-129.

Petters, S. W. (1982). Central West African Cretaceous – Tertiary Benthic Foraminifera and Stratigraphy, Palaeontographica Abteilung A 179, 1 – 104.

Polydorides, N. (2002). Image Reconstruction algorithms for soft-field tomography, Ph.D. dissertation, University of Manchester, Manchester, United Kingdom.

Reijers, T. J. F. (1996). "*Selected Chapters on Geology, SPDC of Nigeria*, Corporate Reprographic Services, Warri, 197p.

Reyment, R. A. (1965). *Aspects of the geology of Nigeria: the stratigraphy of the Cretaceous and Cenozoic deposits.* Ibadan university press. 145p.

Rightmire, C.T., (1984). Coalbed Methane Resources of the United States. AAPG Special Volumes 138, 1–13.

Sada, M. M. (2012, August). Investment opportunities in Nigeria minerals and metals sector. In *Africa Down Under International Conference, Perth, Western Australia*.

Sambo, A. S., Garba, B., Zarma, I. H., & Gaji, M. M. (2010). Electricity generation and the present challenges in the Nigerian power sector.

Samouolian, A., Cousin, I., Tabbagh, A., Bruand, A., & Richard, G. (2005). Electrical resistivity survey in soil science: a review. *Soil and Tillage research, 83*(2), 173-193.

Schnapp, R., & Smith, J. (2012). Coal information. International Energy Agency. Paris.

Schopf, J. M. (1956). A definition of Coal. Society of Economic Geologists, Inc. Economic Geology, v. 51, pp. 521-527.

Sheets, R. A., (2002). Use of Electrical Resistivity to Detect Underground Mine Voids in Ohio. US Geological Survey, Water-Resources Investigations Report 02–4041. https://www.researchgate.net/publication/264380938

Sherrod, L., Sauck, W., & Werkema, J. D. (2012). A low cost, in situ resistivity and temperature monitoring system. *Groundwater Monitoring & Remediation*, *32*(2), 31-39.

Short, K., & Stouble, A. (1967). Outline of geology of Niger Delta. *AAPG bulletin*, *51*(5), 761-779.

Singh K.K.K., Singh K.B., Lokhande R.D. & Prakash A. (2004). Multielectrode resistivity imaging technique for the study of coal seam in northern part of Jharia Coalfield of Dhanbad district. *J. Scient. & Indu. Res.,* 63: 927-930.

Speight, J. G. (2012). *The chemistry and technology of coal.* CRC press.

Speight, J. G. (2015). *Handbook of coal analysis.* John Wiley & Sons.

Stacey, R. W. (2006). Electrical impedance tomography; Technical Report SGP-TR-182;. *The Department of Petroleum Engineering, Stanford University: Stanford, CA, USA.*, 41.

Stovall, J. W. & Brown, H. E. (1955). *The Principles of historical* geology. Ginn.

Stummer P. & Maurer HR (2001). Real-time experimental design applied to high-resolution direct-current resistivity surveys. International Symposium on Optical Science and Technology, Expanded Abstracts, 143-150.

Szalia S., & Szarka L., (2008). On the classification of surface geoelectric arrays. *Journal of Geophysical Prospecting* **56**, 159 - 175.

Tattam, C. (1944). A review of Nigerian stratigraphy. Geological Survey of Nigeria Bulletin, 24, pp. 27-46.

Taylor, G. H., Liu, S. Y., & Diessel, C. F. K. (1989). The cold-climate origin of inertinite-rich Gondwana coals. *International Journal of Coal Geology*, *11*(1), 1-22.

Teichmüller, M., Teichmüller, R., (1968). Geological Aspects of Coal Metamorphism, D. Murchison and T.S. Westoll. ed. Elsevier Publishing Co., New York.

Telford W.M., Geldart L.P., & Sheriff RE (1990). *Applied Geophysics*, Cambridge: Cambridge University Press.

Tiwary, S. N. (1993). Measurement of electrical resistivity of coal samples. *Fuel, 72*(8), 1099-1102.

Tselentis, G. A., & Paraskevopoulos, P. (2002). Application of a high-resolution seismic investigation in a Greek coal mine. *Geophysics*, *67*(1), 50-59.

Tsikritzis, L., Fotakis, M., Tzimkas, N., Kolovos, N., & Tsikritzi, R. (2008). Distribution and correlation of the natural radionuclides in a coal mine of the West Macedonia Lignite Center (Greece). *Journal of Environmental Radioactivity*, *99*(2), 230-237.

Tsourlos, P. (1995). Modelling, interpretation and inversion of multielectrode resistivity survey data. *(Doctoral dissertation, Dept. of Electronics, University of York).*, 315.

Umeji, P. O. (2005). Palynological study of the Okaba coal mine section in the Anambra Basin, Southeastern Nigeria. Journal of Mining and Geology, 4(2): 193-203.

Utom, A. U. (2012). Prediction of shallow aquifer parameters and waterquality in okpara coal mine and environs using geoelectric sounding. *M.Sc Thesis, Nnamdi Azikiwe University, Nigeria.*, 106.

Van Krevelen, D. W. (1957). Coal Science, Aspects of Coal Constitution.

Verma R. K. & Bhuin N. C. (1979). Use of electrical resistivity methods for study of coal seams in parts of the Jharia Coalfield, India. *Geoexploration*, 17: 163-176.

Vickery A, & Hobbs B. (2000). Resistivity imaging to determine clay cover and permeable units at an ex-industrial site. Near Surface Geophysics, 2000; 1: 21 – 30.

Vorres K. S. (1993). *Users handbook for the Argonne premium coal sample program* (No. ANL/PCSP-93/1). Argonne National Lab., IL (United States).

Ward C. R. (2003). Coal exploration and mining geology. School of Geology, University of New South Wales, Sydney, Australia. *Geology*,V: 1 – 9.

Weber, K. J. and Daukoru, E. M. (1975), "Petroleum geological aspects of the Niger Delta", *Journal of Mining and Geology*, 12: 9-22.

Wilkinson, P. B., Loke, M. H., Meldrum, P. I., Chambers, J. E., Kuras, O., Gunn, D. A. andOgilvy, R. D. (2012). Practical aspects of applied optimized survey design forelectrical resistivity tomography, Geophysical Journal International 189 (1), pp. 428-440.

World Coal Institute (2009). *The coal resources: A comprehensive overview of coal* (Research report). Retrived from http://www.worldcoal.org

Wu, G., Yang, G., & Tan, H. (2016). Mapping coalmine goaf using transient electromagnetic method and high density resistivity method in Ordos City, China. Geodesy and Geodynamics, 7(5), 340-347.

Zhou, W., Beck, B., & Stephenson, J. (2000). Reliability of dipole-dipole electrical resistivity tomography for defining depth to bedrock in covered karst terranes. *Environmental geology, 39*(7), 760-766.